Automatic classification of grassland herbs in close-range sensed digital colour images

Dissertation

zur

Erlangung des Doktorgrades (Dr. rer. nat.)

der

Mathematisch-Naturwissenschaftlichen Fakultät

der

Rheinischen Friedrich-Wilhelms-Universität Bonn

vorgelegt am 09.08.2007

von

Steffen Gebhardt

aus

Lutherstadt Wittenberg

Angefertigt mit Genehmigung der Mathematisch-Naturwissenschaftlichen Fakultät der Rheinischen Friedrich-Wilhelms Universität Bonn

1. Referent: Prof. Dr. Walter Kühbauch (em.)
2. Referent: Prof. Dr. Gunter Menz

Tag der mündlichen Prüfung: 26.09.2007

Diese Dissertation ist auf dem Hochschulserver der ULB Bonn
http://hss.ulb.uni-bonn.de/diss_online elektronisch publiziert.
Erscheinungsjahr: 2007

For my parents

The study was accomplished in the second period of the research training group 722 on “Information Techniques for Precision Plant Protection” of the University of Bonn, funded by the German Research Foundation (DFG).

Acknowledgements

It's been a very long journey along to this. A rough path hardly to walk on alone. Thanks to all the people that helped me getting rid of the obstacles.

Thanks to my family and my girl friend. Where would I have gone to without your benefits? Thanks for believing in me and for bearing me (from the financial side of view).

Thanks to Prof. Kühbauch and Prof. Menz for supporting me and encouraging my work and happiness. Thanks to Prof. Thein for joining the dissertation committee. Thanks to PD Dr. Erich-Christian Oerke for the excellent management of the Research Training Group and with that for all the possibilities offered to me.

Special thanks to Dr. Jürgen Schellberg for introducing me to the world of grassland research and for the talks about all the world and his brother. Thanks also for the valuable inputs to my manuscripts.

This work could have never been accomplished without the help of the background people, the technicians and farm workers. Special thanks to Reiner Lock and all the hardworking team players from the University of Bonn Experiment Station Rengen.

Special thanks to Ms. Hiltrud Bartels for all the little things she has done for me which all together form a major part of this work.

Special thanks to Dr. Michael Whiting from the UC Davis for exhaustively reviewing this thesis.

Jonas and Volker, thanks for all the fruitful and honest discussions and comments, even if I didn't want to hear them.

Thanks to all my friends in the world for supporting me in their individual way.

Abstract

The broad-leaved dock (*Rumex obtusifolius* L. (RUMOB)) is one of the most harmful and persistent weed species on European grassland and it has been spread into the temperate grassland regions throughout the world. Large dry matter contributions of *Rumex obtusifolius* L. reduce the quality of the standing forage considerably because of the poor palatability of leaves and tillers and withdraw water and nutrient from surrounding plants. For Central Europe it is estimated that more than 80% of all herbicides used in conventional grassland farming are used to control *Rumex* species. Until today, herbicides are applied over the whole field, even if *Rumex* plants are not homogeneously distributed area-wide.

Recently developed precision farming techniques based on weed mapping that use mainly image processing, enable site-specific spraying of weeds in arable crops. Until today those techniques have not been applied to grassland weed sensing. Compared to the identification of isolated individual plants on a rather uniform soil background in arable crops, image processing for a more complex environment as grassland requires a different approach.

The aim of the thesis was to develop an image processing procedure for automatic detection of grassland weeds using close-range digital colour images, focussing on the detection of RUMOB. A field experiment has been established with grassland plots populated with RUMOB and the other typical broad leaved grassland weeds *Taraxacum officinale* Web. (TAROF) and *Plantago major* L. (PLAMA). Digital colour images have been taken from around 1.5 m above ground at three dates in 2005. Image acquisition was done automatically by a vehicle driven on rails alongside to the experimental plots, whereby nearly constant recording geometry conditions were guaranteed. Images were taken during cloud cover in order to avoid direct sunlight.

Using the images from 2005 an object-oriented image classification has been developed.

Thereby, the leaves of the weeds were separated from the background using parameters of homogeneity and morphology, resulting in a binary image. The remaining image objects in the binary image were contiguous regions of neighbouring pixels related to the object classes of the weed species, soil, and residue objects. Geometrical-, colour and texture features were calculated for each of these objects. Discriminant analysis exhibited that colour and texture features contribute most to the discriminating of objects into the different classes. In a Maximum Likelihood classification these features were used to differentiate the objects into their respective classes. High overall accuracies and even higher RUMOB detection rates were achieved. The algorithm has been modified and applied to images of varying image resolutions. High classification accuracies have been achieved with all image resolutions, whereby the processing time could be improved for images with lowest resolutions.

Images were taken at 13 dates over the two grassland growths in 2006. In all the images the plant species were classified automatically using the developed image classification integrated in a graphical user interface software. The coordinates of the objects classified as RUMOB were transformed into Gauss-Krueger system to generate distribution maps of this weed. The combination of object density and area further decreased its misclassifications. RUMOB classification rates across the season were analysed and phenological stages have been identified on which classification performed best.

The results demonstrate high potential of machine vision for weed detection in grassland. A classification procedure based on image analysis and Geographic Information System (GIS) post-processing has been developed for detecting *Rumex obtusifolius* L. and other weeds in grassland with high accuracy. Future projects might focus on the application to real grassland conditions and the derivation of RUMOB distribution maps. Thus, herbicide application maps can be calculated, utilized for site-specific weed control. The development of an image acquisition unit to be mounted on a driving vehicle along with a standardization of image recording is going to be the main focus.

Contents

1. Introduction

1.1. Impact of *Rumex obtusifolius* L. (broad-leaved dock) on grassland

The broad-leaved dock (RUMOB) (Figure 1.1) is considered as one of the five most widely distributed non-cultivated plant species in the world (Zaller, 2004). RUMOB is found in European grasslands and has been spread throughout the world (Cavers & Harper, 1964). It is found in many widely different plant communities including woods, arable fields, grassland and waste places. Cavers and Harper (1964) reported that for the growth of this species apparently no climatic limitations exist. As a 'follower of men' its absence from high altitude areas is probably caused by the lack of disturbed ground on these heights (Cavers & Harper, 1964). The species is present on almost all soil types but less often on peat and rarely on acid soils (Zaller, 2004; Cavers & Harper, 1964).

Rumex obtusifolius L. competes with sown and native pasture species, and arable crops; occupying area which could be utilized by more palatable species (Zaller, 2004). The availability of large concentrations of soil nutrients, especially nitrogen, increases its competitiveness. Open spaces in damaged grazed swards, high nutrient availability and liquid manure, and high animal stocking rates improve the conditions for reproduction, germination and rapid expansion of RUMOB. When harvested with forage, silage, and hay the cattle assimilate the seeds, which persist in the rumen, as well as in slurry and farmyard manure, and remain viable throughout hard winters in the sward and soil.

The life cycle of *Rumex obtusifolius* L., adopted from Elsässer (2004), is illustrated in Figure 1.2. RUMOB has low competitive ability as a seedling and hardly becomes established in closed communities (Cavers & Harper, 1964). Although once it has produced a deep spreading

Figure 1.1.: *Grassland field infested with Rumex obtusifolius at the University of Bonn Grassland Farm in Rengen, Germany.*

tap root it is a most troublesome weed and is very difficult to eradicate. By its widely ramified root systems plants of RUMOB withdraw water and nutrient from surrounding plants. Pieces of the underground stem can quickly regenerate from dissected roots after ploughing (Cavers & Harper, 1964). New shoots are quickly sent up from ground level. It then has a great advantage over the shallower-rooted perennial grasses (Zaller, 2004; Cavers & Harper, 1964). High plant density of RUMOB significantly reduces the average quality of the standing forage due to the poor palatability of leaves and tillers. Besides the low palatability, it favours digestive problems due to contents of oxalic and silicic acids and tanning agents. Once established in grassland, plants tend to flower freely for several years. The combination of flowering several times a year, producing a large number of seeds (up to 60.000 seeds per plant) that remain viable in the

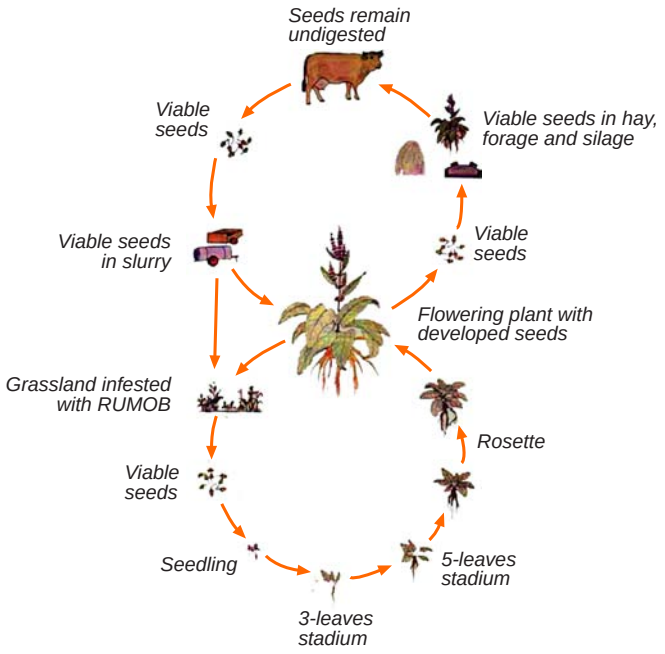

Figure 1.2.: *The life cycle of Rumex obtusifolius. Adopted from Elsässer (2004).*

soil for many years, the ability to quickly establish from seeds and the low seedling mortality, makes RUMOB a successful weed on agricultural land (Zaller, 2004; Cavers & Harper, 1964).

It is not possible to suppress established RUMOB plants by pasture management practices, such as cutting frequency, N dosage, or modifying the botanical composition, even when the competition from neighbouring species is very strong (Niggli, 1985). To achieve lasting improvements in the botanical composition of the plant stand, specific interventions are needed (Niggli, 1985). Necessary preventive actions include: (1) maintaining well-balanced fertilization; (2) avoid sod opening and closing of gaps immediately; (3) cutting grassland before plants flower; (4) apply control practices early. In organic farming, individual plants of RUMOB are controlled through manual weeding, either by hand or mechanical digging. Each individual plant must be detected by the worker and cut from the sod using specific spades. Recent developments aim to replace the manual digging by machines. However, still a worker is required for guiding the machine to each plant. The operation remains exhausting and the machines

leave unacceptable damage to the field. Those methods are time consuming and expensive.

In Central Europe approximately 80% of all herbicides used in conventional grassland farming are used to control *Rumex* species (Galler, 1989). The optimal time for chemical control is when the plant has completely developed its rosette, preferably in the late summer and autumn before temperatures are below 25°C. While each individual RUMOB plant of is harmful, the reported weed thresholds for controlling are very low. For example, the chamber of agriculture (Landwirtschaftskammer) Niedersachsen, Germany, defines the thresholds as: 5% of the grassland fields infested with RUMOB or 3 - 5 RUMOB plants per 10 m^2 (Hoppe, 2007). The Swiss consortium on the promotion of crop production (AGGF) recommends that the chemical control of RUMOB shall be carried out plant individually if only few weeds appear in the field. However, if abundance of RUMOB increases 1 plant per m^2 herbicides shall be applied over the whole field (Kessler & Ammon, 1996; Zwerger & Ammon, 1999). Using for example the Asulam herbicide best efficiency is achieved when the RUMOB rosette is fully established either in the spring growth or in autumn (starting in late August). Amidosulfuron shall be applied in late summer to autumn (Zwerger & Ammon, 1999).

Elementary rules in chemical weed management are: (i) to favour site-specific management over whole field treatment, (ii) use of permitted selective herbicides only, (iii) application at the right time, when leaf area is fully developed and before blossoming and on dry days, (iv) to keep the recommended waiting period after application, and (v) to close occurred gaps in the grass sod after application (Pötsch, 2001).

1.2. Precision agriculture for weed management

Weeds do not grow uniformly; there is significant spatial variability in weed plant density and in weed type across a field (Lamb & Brown, 2001). For operational effectiveness however, the normal practice of farmers is to spray the entire field at a uniform rate (Stafford & Miller, 1993).

Studies in arable crops, driven by the idea of precision farming and spatially variable chemical application, specifically “patch spraying technology” have provided quantitative data concerning the degree of patchiness of a number of specific weeds (Gerhards *et al.* , 1997; Dicke *et al.*

, 2007). There is a great potential in saving herbicides by targeting applications and vary the application rate to the weed density. Such precision farming techniques enable the reduction of herbicides, along with reduced management costs and environmental friendliness (Gerhards *et al.* , 2000; Thorp & Tian, 2004; Gerhards & Oebel, 2006).

The basis for site-specific weed control is to know where the weeds appear in the field. Weeds mapped on a field scale give farm managers the ability to monitor the effectiveness of weed management strategies and to ascertain the chemical requirements of spraying (Lamb & Brown, 2001). Weed maps provide the navigation source for sprayers guided by a Global Positioning System (Stafford *et al.* , 1996; Gerhards *et al.* , 1997; Dicke *et al.* , 2004; Dicke *et al.* , 2007).

In the past, most field-scale weed maps have been constructed from on-ground survey techniques, for example GPS-assisted field walking (Stafford *et al.* , 1996) or grid sampling (Dicke *et al.* , 2007). They are of limited use for commercial weed management, because of issues such as field mobility, cost, labour and time (Lamb & Brown, 2001). Remote sensing of weeds using either satellite- or airborne sensors offer a more sophisticated possibility to detect weeds in the field and to derive weed distribution maps. These approaches for weed mapping work offline and require four fundamental steps which are: (1) images acquisition; (2) images classification; (3) derivation of weed distribution and herbicide application map; and (4) spraying herbicides according to the herbicide application map. Close-range imaging is potentially suitable for online systems for weed management with sensors mounted at the front of the tractor and the data classified real-time with on board computers to direct the herbicidation (Marchant *et al.* , 1998).

1.3. Remote sensing of weeds

Remote sensing offers an non-invasive method for detection and mapping of weeds. The two requirements necessary for remote sensing of weeds are: (i) suitable differences in spectral reflectance or texture exist between weeds and their background soil and plant canopy, and (ii) the remote sensing instrument has appropriate spatial and spectral resolution to detect weed plants (Lamb & Brown, 2001).

Airborne remote sensing platforms have been used for weed detection since the early 1980s

(Thorp & Tian, 2004). Multi- and hyperspectral imaging sensors as well as video cameras were utilized for weed, crop, soil, and residue discrimination in arable crops (Menges *et al.* , 1985; Richardson *et al.* , 1985; Thorp & Tian, 2004; Lopez-Granados *et al.* , 2006). These systems depend on differences in the spectral signatures for pixel-based thematic classification.

The separation of crop and weeds from background is much more complicated in range- and grasslands than in fields with uniform crop cover. However, flowering stages of some weeds exhibit spectral signatures significantly different from surrounding grasses which improves weed detection using aerial multispectral video and photography (Everitt *et al.* , 1984; Everitt *et al.* , 1987; Everitt *et al.* , 1992; Everitt *et al.* , 1995) and hyperspectral data (Glenn *et al.* , 2005). Also, satellite sensors have been used to detect large aggregations of weeds (Everitt *et al.* , 1993; Thorp & Tian, 2004). All the above mentioned studies, using either airborne or satellite remote sensing data are not suitable to detect individual plants and to distinguish between weed species and crops, because of the insufficient spatial resolution and similar spectral properties of weeds and crops. For example, Lamb *et al.* (1999) have mapped continuous populations of *Avena* sp. in a field of seedling triticale undersown with clover using 0.5, 1.0, 1.5, and 2.0 m resolution multispectral imagery. The highest resolution imagery was able to discriminate the lowest weed densities of 17 plants/m^2 from the seedling crop, soil background. Below that weed density, inter-row weeds could not be reliably distinguished from the background.

Due to the low spatial resolution present satellite and airborne remote sensing capability is limited to the detection of aggregated weed patches only. In contrast to close-range sensors, the image classification is limited to pixel-based classification using the spectral information of each pixel.

Sensor platforms at low altitudes, for example drones, balloons, or ground-based sensors, can overcome the spatial resolution limitations. Greater proximity reduces the pixel sizes to millimetres or smaller. In the past, researchers have approached ground-based weed sensing in arable crops using machine vision technology (Thorp & Tian, 2004), with the benefits of both image analysis methods, pixel-based and object-oriented classification. In object-oriented image classification, contiguous regions of neighbouring pixels are classified instead of single pixels. With sufficient spatial resolution (below 1 mm) images collected with ground-based camera systems and subsequent image processing routines enable to segment vegetation from

soil background and delineate individual weeds from crop (Thorp & Tian, 2004). Soil and vegetation are thereby separated based on differences in colour (Woebbecke *et al.* , 1995a; Marchant *et al.* , 1998; Tian & Slaughter, 1998; Soille, 2000; Hemming & Rath, 2001; Perez *et al.* , 2000) or in the red and infra-red reflectance (Brivot & Marchant, 1996; Lamb & Brown, 2001; Gerhards *et al.* , 2002; Thorp & Tian, 2004). In a two step agricultural machine vision application, vegetation is separated from soil background, then weeds are distinguished from crop, using spectral, spatial, and/or textural information within images (Thorp & Tian, 2004; Perez *et al.* , 2000; Kavdir, 2004; Aitkenhead *et al.* , 2003; Marchant & Onyango, 2003; Brivot & Marchant, 1996; Onyango *et al.* , 2005; Tillett *et al.* , 2001; Hemming & Rath, 2001).

Spectral object properties have been used to identify weed seedlings (Franz *et al.* , 1991b), weeds having reddish stems (Zhang & Chaisattapagon, 1995), and to discriminate weeds from corn plants (Jia & Krutz, 1992). Determining shape parameters were successfully used to discriminate between different weed species (Petry & Kühbauch, 1989; Franz *et al.* , 1991a; Woebbecke *et al.* , 1995b; Neto *et al.* , 2006). However, this fails when plant leaves overlap. The third method for discrimination of plant species in ground-based weed detection applications involves the measurement of the textural appearance of a plant or plant canopy as a whole (Thorp & Tian, 2004). For example, Burks *et al.* (2005), Shearer and Holmes (1990), and Meyer *et al.* (Meyer *et al.* , 1998) determined textural features from the colour co-occurrence matrices to discriminate weed species.

Lamb and Brown (2001) and Thorp and Tian (2004) provide two very detailed reviews on literature about the remote sensing of weeds.

Since these studies were conducted on arable crops, the separation of weeds from soil is somewhat easier than in range land or grassland.

1.4. Objectives of the study

As mentioned above, the potential of image classification for grassland weed detection has not been investigated and would promote precision farming techniques in grassland farming. The aim of the study was to investigate the potential of close-range remote sensing colour images for detecting weeds in grassland. In particular it focused on the identification of one

of the most invasive and persistent weed species on European grassland, the broad-leaved dock (*Rumex obtusifolius* L., RUMOB). Future practical applications on permanent grassland require systematic studies on plant discrimination in mixed swards. Aim of this study was the development of image classification algorithms to accurately recognize RUMOB in mixed permanent grassland swards, including distinguishing from herbs frequently associated with RUMOB, such as TAROF and PLAMA.

Based on images taken during 2005 and 2006 four experiments were conducted. Experiments 1 to 3 deal with the creation and improvement of an image classification algorithm for RUMOB detection and the investigation of the influence of image resolution on classification accuracy. In the fourth experiment the image classification results were transformed to distribution maps of RUMOB. Misclassification was further reduced by combining object area with object density before deriving herbicide application maps. Additionally, time optimal periods and plant growth stages across the grassland growing season were identified suitable for RUMOB mapping. An introductory summary of each experiment is given below:

Experiment 1: Suitability of close-range sensed colour images and object-oriented image classification for the detection of broad-leaved dock (*Rumex obtusifolius* L.) within mixed grassland swards.

This base study focussed on the applicability of ground-based colour images and subsequent image classification for weed detection in grassland. At three dates in July 2005, 108 digital photographs were obtained from a field experiment that is described below. An object-oriented image classification algorithm was developed. To segment the red, green, blue (RGB) colour images they were transformed to grey scale intensity images in a first step. Based on that, local homogeneity images were calculated and a homogeneity threshold was applied to generate binary images. Finally, morphological opening (image erosion followed by dilation) was performed. Shape, colour and texture features were calculated for each of the objects remaining after image segmentation. Based on these features, a Maximum Likelihood classification was done to discriminate RUMOB from other herbs and the soil background. Rank analysis was used to evaluate the influence that combinations of features had on the classification result.

Experiment 2: An extended algorithm for automatic *Rumex obtusifolius* detection using colour and textural object features.

This section describes an improved algorithm that increases classification accuracy and reduces confusion of other weeds. The leaves of RUMOB, TAROF, PLAMA, and other homogeneous regions were segmented automatically in the digital colour images using local homogeneity and morphological operations as in the first experiment. Additional texture and colour features were identified that contribute to the differentiation through a stepwise discriminant analysis. Again, Maximum-likelihood classification was performed based the variables retained after discriminant analysis. The results were compared to those of the first classification algorithm.

Experiment 3: The influence of image resolution on the classification accuracy

Experiments 1 and 2 were performed on eight million pixel images. Processing of these images, particularly image segmentation, is rather slow, taking up to one minute per image. Reducing of image size would speed up processing time, however what impact would decreasing image resolution have on the classification results? The eight million pixel images were resampled to create images at six decreasing resolutions, determining the resolutions of typical industrial cameras. Processing results of these images were compared to determine the best resolution, in terms of classification accuracy and processing times.

Experiment 4: Continuous mapping of *Rumex obtusifolius* during different grassland growths based on automatic image classification and GIS-based post processing

This experiment combines the results of the object-oriented image classification with geospatial post-processing. Images acquired at 13 dates during two grassland growths in 2006 were classified automatically. Image objects classified as RUMOB were mapped to a cartographic coordinate system using coordinate transformation to create weed distribution within GIS. Finally, object density and area were combined to improve detection accuracy and to derive herbicide application maps. Both, the distribution and herbicide application maps, were compared to the setup of the observed grassland plot experiment. Further, the best time periods to achieve high classification accuracies were determined. From this the phenological stages

of RUMOB plants were identified for recommending the appropriate point for the automatic weed mapping.

1.5. Field experiment

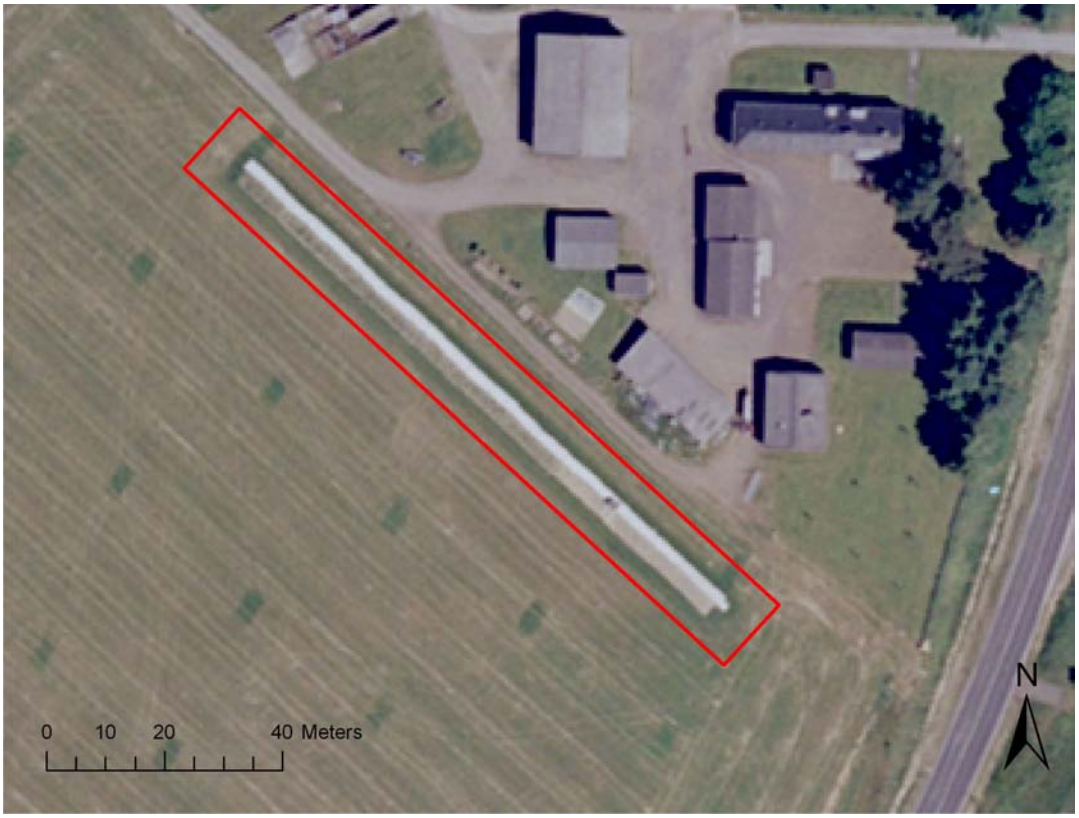

Figure 1.3.: *Aerial photograph of the experimental site at the University of Bonn Experiment Station Rengen taken on June, 19th in 2005. Photo is courtasy of Landesamt für Vermessung und Geobasisinformation Rheinland-Pfalz, Germany. 24.01.2007; Az.: 26 722-1.51*

Investigations on the contribution of machine vision for weed detection require standardised setups of plant growth and plant communities. Respective experiments can be set up either in greenhouses or on field experiments. In greenhouses, however, plants grow different to those under field conditions due to other environmental conditions. To overcome these limitations, field experiments are required which enable the monitoring of growing plants under natural conditions, but in a standardized manner.

For this study, a field experiment was set up in spring 2005 at the University of Bonn Experiment Station Rengen in the Eifel mountains, Germany, about 60 km west of the Rhine river (50°13' N, 6°51' E) at 475 m a.s.l. The mean annual precipitation is 811 mm with a mean

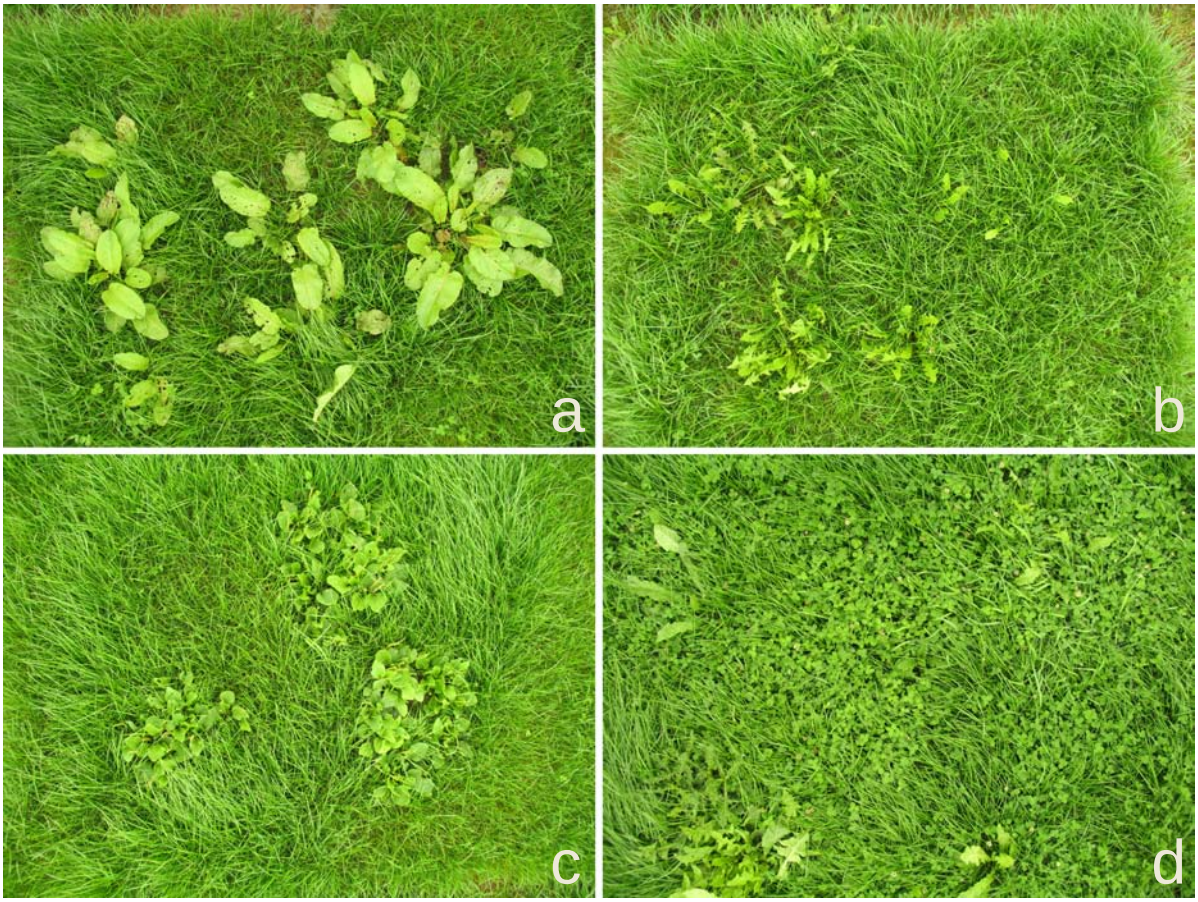

Figure 1.4.: *Species planted within the experimental plots: (a) Rumex obtusifolius L., (b) Taraxacum officinale Web., (c) Plantago major L., (d) Trifolium repens L.. Images were captured on August, 15th in 2006.*

annual temperature of 6-9°C (1934-91). The soil has been characterized as a pseudo-gley.

The experimental field enclosed a row of 54 plots. Each plot area was around 2.7 × 2 m, hence the experiment was around 110 meters long. The annotated aerial image taken on June, 19th in 2005 in Figure 1.3 shows the experiment.

On 36 of these plots sods of rye grass (*Lolium perenne* L.) were established. On the remaining 18 plots bare soil background was kept. From the plots with rye grass 18 were established without gaps, whereas on the other 18 plots mechanically added gaps were introduced showing the bare soil background.

When talking about weed detection in grassland we cannot talk about RUMOB exclusively,

Figure 1.5.: *Planting setup: (a) non-overlapping individuals of one species, (b) overlapping individuals of one species, (c) mixture plot with all species. Images were captured on August, 15th in 2006.*

even if it is one of the most harmful. There are certain other typical broad-leaved herbs in European grasslands which might be confused with RUMOB even if they are not necessarily harmful or are actually wanted in grasslands (e.g. *Taraxacum officinale* Web. and *Trifolium repens* L.). Therefore, together with RUMOB, three more herb species, *Taraxacum officinale* Web. (TAROF), *Plantago major* L. (PLAMA) and *Trifolium repens* L. were grown in the greenhouse and then transplanted into the experimental plots in May 2005. Figure 1.4 shows monitored experimental plots with the established herb species, captured on August, 15th in 2006. To enable the detection of non-overlapping plant individuals only, these species were planted in plots 1 to 8 at distances far enough apart to avoid overlap (Figure 1.5a). In contrast to the first eight plots, in the plots 9 to 16 the above species were planted close enough to allow overlap (Figure 1.5b). Each plot was planted with only one species, whereas in plots 17 and 18 a mixture of overlapping individuals of all the above mentioned species was established (Figure 1.5c). This method of planting the four species in plots 1 to 18 was repeated for the remaining 36 plots (19 to 54). The setup of the whole experiment is shown in Figure 1.6.

Nitrogen fertilization at a dosage of 80 kg/ha was applied right after the weeds were planted in and again directly after cutting all plots on July 11th, 2005.

It has to be mentioned here, that for the 18 plots with bare soil background no contribution to the classification approach was found and hence with these 18 plots remained unused in 2005. The images of these plots required an different approach for image segmentation than those plots with grass sod. Therefore, in autumn 2005 *Lolium perenne* L. was sown into these plots as well, giving a total of 54 grassland plots. The experiment was repeated in 2006, whereby two

grassland growths were monitored. The first grassland cut was on May, 4th while the second cut was conducted on July, 6th, at a cutting height of 7 cm. In each of the two growths, all 54 plots have been fertilized with nitrogen at a dosage of 80 kg/ha directly after cutting.

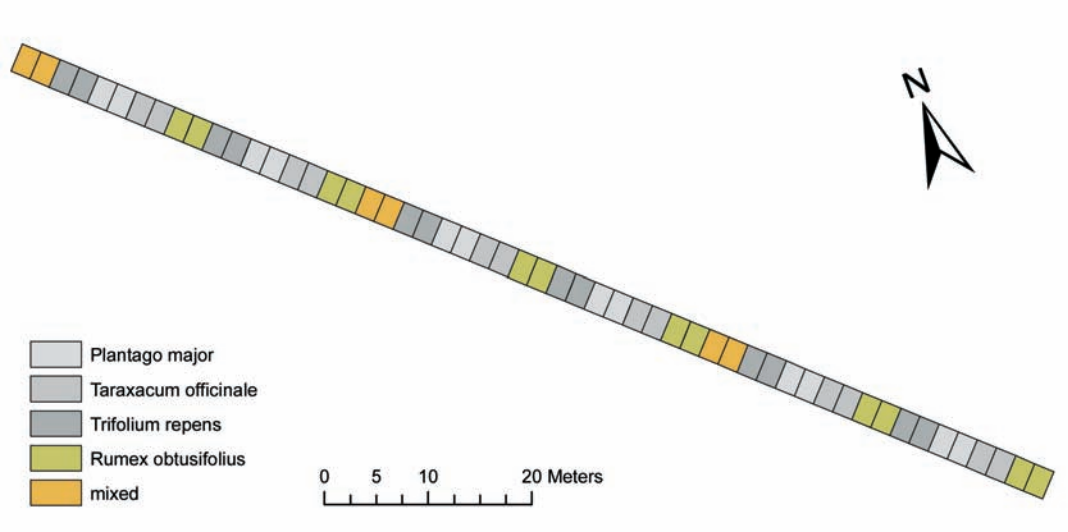

Figure 1.6.: *Setup of the grassland experiment with 54 plots established at the University of Bonn Experiment Station Rengen. Four typical dicot herbs of European grasslands have been planted into the plots either individually or mixed.*

1.6. Image acquisition

The image recording was done in close-range from about 1.60 m above ground by an autonomous vehicle (Figure 1.7), driven on rails about 110 m long parallel to the row of plots. The vehicle consisted of a chassis and a rotary arm perpendicular to the driving direction. The 4-wheel chassis was equipped with the batteries for power supply, 4 electronic motors, light barriers for guiding the vehicle to the plots and an electronic control box that contains the hardware and software to manage the movement, positioning and control of the vehicle. The camera was mounted on the rotary arm adjusted nadir looking to the plot's centerline. Guided by the electronic light barriers the vehicle stops automatically at the centre of each plot. At this point the camera was released remotely, and images of every plot were recorded separately. The captured images covered almost the whole plot. The system needed 20 minutes for photographing all experimental plots. The images were taken on daytime. To avoid light reflectance and shadows in the plots induced by direct sunlight, images were taken only under diffuse illumination conditions. Prior to recording a set of images of all experimental plots a manual white balance was applied. Even if the illumination condition changed a little within the 20 minutes of recording, the white balance ensured an almost constant measuring of the colours in all images and with that a good image quality.

The utilized camera was a Canon Powershot Pro1 (Canon, Inc.), which is an compact digital still colour (RGB) camera. This camera features an eight-megapixel Charge-Coupled Device (CCD) image sensor, and a built-in Canon Luxary Lens. The lens realizes a 7× (equivalent to 28-200mm in 35mm format) optical zoom ratio with an aparture speed range of f/2.4-3.5. For image acquisition the sensitivity was set to ISO International Organization for Standardization 100. Exposure time was calculated automatically by the camera. The focal length was set to endless. Auto focus was enabled. With the full resolution of 3264 × 2448 pixels and the camera height above the surface the pixel size was approximately 0.6 × 0.6 mm at the image center. To avoid loss of quality, the images were stored as uncompressed Canon RAW files om compact flash card and transformed to Tagged Image File Format (TIFF) thereafter.

The advantage of this system are the almost constant recording geometry conditions and the automatic image acquisition.

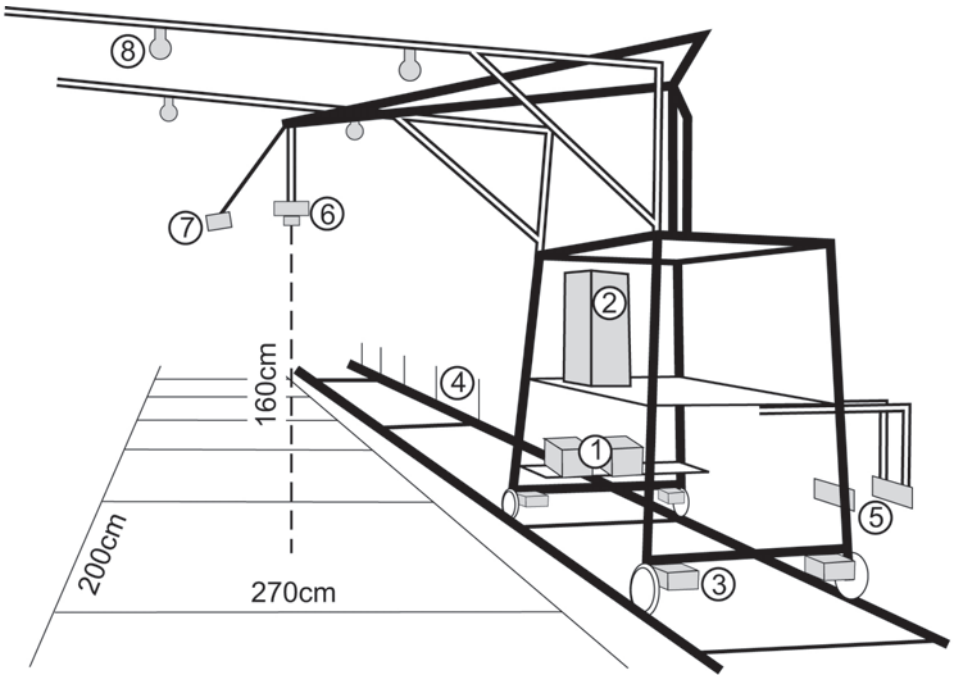

Figure 1.7.: *Technical setup of the image acquisition in the field. The vehicle is power supplied by 12V batteries (1). The electronic control box (2) contains the hardware and software to manage the movement, positioning and control of the vehicle. Four electronic motors (3) move the vehicle forward which automatically stops when a positioning stick (4) at each treatment is suspending the electronic light barrier (5). At each stop, the camera (6) is released through a remote control (7). Electric light sources (8) allow image recording at night times under controlled illumination conditions.*

In 2005, images were recorded on July 19th, 22nd, and 28th, which equals Day Of Year (DOY) 200, 203, and 209, respectively. Hence, 162 images were collected. The two grassland growths in 2006 were monitored at 13 dates from May until September. In the first growing period, images were taken at May 23rd and 29th, June 14th, 20th, and 26th and July 5th (DOYs 143, 149, 165, 171, 177, 186). The regrowth of the grass plots was covered by images taken on July 11th, 20th, and 31st, August 15th and 29th, and September 8th and 12th (DOYs 192, 201, 212, 227, 234, 251, 155) in 2006. A total of 702 images were acquired.

2. Suitability of close-range sensed colour images and object-oriented image classification for the detection of *Rumex obtusifolius* within mixed grassland swards

2.1. Introduction

The detection of individual weed plants is unlikely to be successful with far-range-remotely sensed image data because of inadequate spatial resolution. Therefore, image analysis has been introduced to close-range photographs to detect weeds in arable crops mainly.

To date little research has been done on vegetation classification in grassland using near-range imagery. Tamura *et al.* (2000) described a method to distinguish clover and gramineous weeds by applying a micro-shape based feature extraction method. Using images of clover, gramineous weeds and bare ground as training sections, they defined nine micro shape textures that could be extracted using a bank of non-linear filters of several sizes. They derived linear discriminant functions for classification, and 98% of the training sections and 88% of the test sections were classified correctly. Bonesmo *et al.* (2004) developed an image processing system to estimate the canopy cover of white clover in a grass-clover mixtures, based on clover colour and morphological properties. The efficiency of the system was tested in the field. The regression coefficient between the canopy cover of clover estimated by image processing and that estimated by manually marking the clover patches was 0.82. However, non of these studies

focussed on weed identification.

This analysis focusses on the testing of ground-based colour images and subsequent image classification for detecting herbs in mixed experimental grassland plots, focussing one of the most harmful weed, *Rumex obtusifolius* L..

2.2. Image classification procedure

2.2.1. Materials and methods

The development of the subsequent image classification procedure was based on the 108 images taken at three dates in July, 2005. An object oriented image classification was applied to the images, which is a common application of pattern recognition in machine vision. The steps required for this are: (1) image acquisition, (2) pre-processing and image segmentation, (3) feature extraction and (4) classification (Gonzales & Woods, 1992; Duda *et al.* , 2001). Image objects, which are contiguous regions of neighbouring pixels that were extracted in the image segmentation step, were classified rather than single pixels. These objects were classified using their mathematical pattern, which is a vector of information comprising their geometry, colour and texture. In contrast, pixel-based image classification uses the spectral information in one or more spectral bands, and attempts to classify each pixel based only on this information. In the following paragraphs the performed processing steps are described.

2.2.1.1. Pre-processing and image segmentation

All image processing steps were applied or developed within Mathworks MATLAB (© The MathWorks, Inc.) using the MATLAB Image Processing Toolbox. In a pre-processing step, the images were converted from 24-bit red, green, blue (RGB) images to 8-bit intensity images using standard formula, Eq. (2.1), which is the National Television System Committee (NTSC) of the United States of America standard for luminance,

$$I = 0.2989 \bullet R + 0.587 \bullet G + 0.114 \bullet B \tag{2.1}$$

where R, G and B is the pixel intensity in the red, green, and blue channel, respectively, and I is the intensity of the resulting grey scale pixel. The intensity depends strongly on the

illumination conditions. However, constant measurement conditions (see chapter 1.6) in this experiment ensured nearly equal I values, thus enabling simultaneous processing of all images without illumination interference.

The aim of image segmentation is to locate certain objects of interest, which, in this case, were the leaves of the weeds. The procedure detects contiguous regions in an image by merging neighbouring pixels using a defined criterion. The texture of the leaves of RUMOB and accompanying herbs were identified as more homogenous than those of grass. A measure of homogeneity was used to separate the leaves of the herbs and of RUMOB from the background. The local homogeneity was calculated according to Cheng and Sun (Cheng & Sun, 2000). First, the standard deviation image of I was calculated by

$$S_{ij} = \sqrt{\frac{1}{n_W} \sum_{I_W \in W_d(P_{ij})} (I_W - m_{ij})^2} \tag{2.2}$$

where S_{ij} is the standard deviation at the central pixel P_{ij}, m_{ij} is the mean of n_W intensities I_W within the window $W_d(P_{ij})$ of $d \times d$ pixel size with $d = 5$ in this case, n_w is the number of pixels within the 5 × 5 pixel window W. The gradient $G_{x_{ij}}$ (in direction x) as well as $G_{y_{ij}}$ (in direction y) was calculated as a measure of the change of grey values at pixel P_{ij} by applying the Sobel-operator Equations (2.3) and (2.4) to the intensity image I.

$$G_{x_{ij}} = \begin{bmatrix} -1 & 0 & 1 \\ -2 & 0 & 2 \\ -1 & 0 & 2 \end{bmatrix} \bullet W_d(P_{ij}) \tag{2.3}$$

$$G_{y_{ij}} = \begin{bmatrix} 1 & 2 & 1 \\ 0 & 0 & 0 \\ -1 & 2 & 1 \end{bmatrix} \bullet W_d(P_{ij}) \tag{2.4}$$

The gradient magnitude ∇f is calculated by Equation (2.5) (Gonzales & Woods, 1992). The gradient is large where the maximum grey level range within the 3 × 3 window $W_d(P_{ij})$ is maximum and low where the grey levels are approximately the same.

$$\nabla f_{ij} = \sqrt{G_{x_{ij}}^2 + G_{y_{ij}}^2} \tag{2.5}$$

The local homogeneity H_{ij} is calculated using the maximum normalized gradient and standard deviation images $\nabla f_{ij}/\nabla f_{ij_{max}}$ and $S_{ij}/S_{ij_{max}}$, respectively.

$$H_{ij} = 1 - \frac{\nabla f_{ij}}{\nabla f_{ij_{max}}} \bullet \frac{S_{ij}}{S_{ij_{max}}} \tag{2.6}$$

By definition, the H_{ij} value ranges from zero to one. Pixels with a local homogeneity close to one were considered to be within homogeneous regions, and vice versa. A binary image B_{ij} was derived from the local homogeneous image by applying a threshold to H_{ij}.

$$B_{ij} = \begin{matrix} 0 & if & H_{ij} < 0.97 \\ 1 & & otherwise \end{matrix} \tag{2.7}$$

A threshold value of $H_{ij} < 0.97$ was identified empirically and performed best in terms of detecting homogeneous regions. As a final image processing step, morphological opening (Gonzales & Woods, 1992) was performed on the binary image B_{ij} using Equation (2.8) with a diamond structure element (S) of radius three pixels. The opening is an erosion $E(B_{ij}, S)$ of image B_{ij} by S, followed by a dilation $D(E(B_{ij}, S), S)$ of the result by S. The resulting binary image now consisted of several white objects (e.g. weeds) with grey level 1 and a background object with grey level 0.

$$O(B_{ij}, S) = D(E(B_{ij}, S), S) \tag{2.8}$$

As the leaf size of RUMOB and the other weeds differed markedly from the background, an area threshold helped to discriminate them from smaller objects in the binary image, such as grass and clover. An area threshold of 5000 pixels which represents about 17 cm^2 on the ground was applied. The leaves of RUMOB covered larger areas than this threshold for all recording dates. The constancy of scale and geometry for all images allowed the area of the objects to be calculated based on the number of pixels within each object. Hence, a transformation of the image coordinate system to a metric one was unnecessary. An example of image segmentation is shown in Figure 2.1. The preceding image processing steps enabled the segmentation of leaves from the grass background. These leaves were represented as clusters (contiguous regions) of foreground pixels which are defined further on as objects.

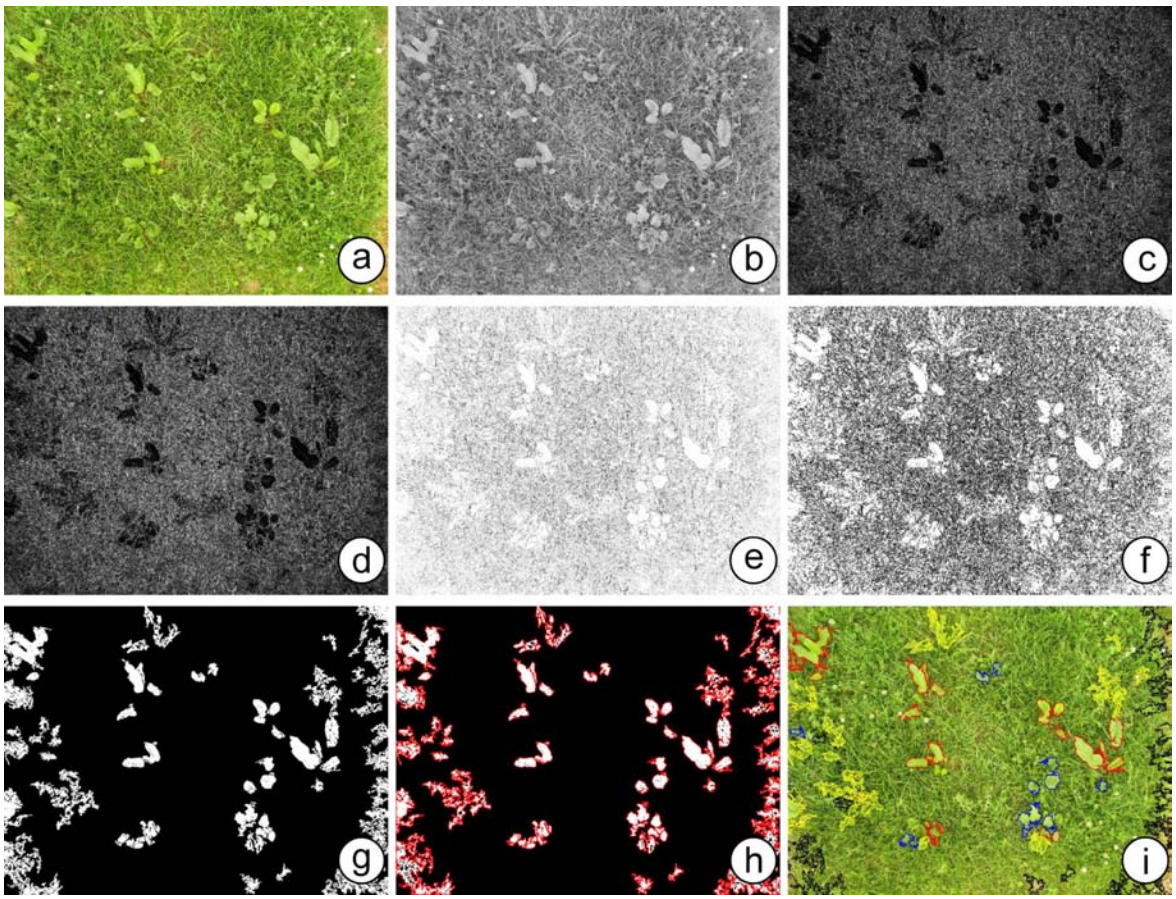

Figure 2.1.: *Image segmentation procedure and example of classification result: (a) the original red, green, blue (RGB) image, (b) the intensity image calculated from (a), (c) the gradient image derived from (b), (d) the standard deviation image derived from (b), (e) the local homogeneity image calculated from (c) and (d), (f) the binary image after applying the grey-level threshold to the local homogeneous image and eliminating objects smaller than 5000 pixels, (g) the final binary image derived by morphological opening of (f) and eliminating objects smaller 5000 pixels, (h) the objects contours and (i) classification result.*

2.2.1.2. Feature extraction

Feature extraction aims to describe the properties of objects mathematically. Specific features suitable for separating RUMOB from the remaining object classes needed to be identified. Visual observations indicated that the leaf shape of RUMOB differed from those of the other herbs. Consequently, the aim was to identify geometrical features describing these shapes (Du & Sun, 2004). The simplest features that could be extracted were *Area* and *Perimeter*. The *Shape Factor* gives information about the compactness of the shape of the object; the most compact shape is a circle (*Shape Factor* = 1). The *Shape Factor* decreases when the perimeter increases and the area remains constant, for example the leaves of *Taraxacum officinale* have a jagged outline. Another parameter describing compactness is *Circularity*, which is 4 for a circle and which increases with increasing perimeter for a nearly constant area.

$$ShapeFactor = \frac{4\Pi * Area}{Perimeter^2} \tag{2.9}$$

$$Circularity = \frac{Perimeter^2}{Area} \tag{2.10}$$

The *Eccentricity* was calculated from the ratio of the semi-minor and semi-major axes of the surrounding ellipse.

$$Eccentricity = \sqrt{1 - \frac{SemiMinor^2}{SemiMajor^2}} \tag{2.11}$$

The *Eccentricity* ranges from zero for a circle to almost one for a thin ellipse. In this approach, *Area* and *Perimeter* are not invariant in relation to scale, but we could disregard this as all images were recorded at the same scale. The geometric representation described here provided a feature matrix containing as many feature vectors as objects in the images, including the vector elements *Area*, *Perimeter*, *Shape Factor*, *Circularity* and *Eccentricity*. Objects derived from image segmentation were not always leaves, but also homogeneous soil objects, which could not be described and discriminated from leaves by their shape alone. Therefore, colour features of the objects were calculated as well. The mean values of intensity (μ_I), as well as the mean grey values of red (μ_R) and green (μ_G) channels in the original RGB image were derived for each object using Equations (2.12)-(2.14). According to Soille

(Soille, 2000) the blue channel contributes little to discriminate soil from vegetation and so was disregarded. Veins on the upper side of RUMOB leaves and the herbs give rise to different degrees of surface roughness. Therefore, the mean value of the gradient ($\mu\nabla f$) computed by Equation (2.15) within an object was included in the feature extraction as a measure of the surface roughness.

$$\mu_I = \frac{1}{n}\sum_{i=1}^{n} I_i \tag{2.12}$$

$$\mu_G = \frac{1}{n}\sum_{i=1}^{n} G_i \tag{2.13}$$

$$\mu_R = \frac{1}{n}\sum_{i=1}^{n} R_i \tag{2.14}$$

$$\mu_{\nabla f_i} = \frac{1}{n}\sum_{i=1}^{n} \nabla f_i \tag{2.15}$$

where n is the number of pixels within an object, and I_i, G_i, R_i, $\mu\nabla f_i$ are the values for intensity, green, red and gradient in an object at the position i, respectively. The feature matrix was extended by including the means of I, G, R and ∇f resulting in a total of nine vector elements. Six feature matrices were calculated from six available sets of data obtained for three recording dates.

2.2.1.3. Classification

A Maximum Likelihood Estimation (MLE) (Stork *et al.* , 2004) was used to classify the objects into a defined number of classes i, which was either i=5 (RUMOB, TAROF, PLAMA, soil and residue) or i=2 (RUMOB and residue). The MLE is a parametric classification method. Each class ω_i is represented by a parameter vector θ_i. These parameters are calculated using a set of sample objects with known group membership called the training dataset. The calculation of these parameters is the training of the classifier.

There were marked morphological changes in the plant organs over time. Therefore, the aim was to determine whether the time span between establishing the training data set and obtaining the data to be classified had any influence on the result. The classifier was trained

using subsets of the feature matrices obtained from data recorded on July 19th and July 22nd, and the corresponding classes for i=5 and i=2 were assigned manually. The first training data set had 209 objects (45 RUMOB, 29 TAROF, 50 PLAMA, 22 soil, 63 residue for i=5 and 45 RUMOB plus 164 residue for i=2). Then a new training data set was created using the feature matrix of July, 22nd including 252 objects (55 RUMOB, 37 TAROF, 43 PLAMA, 39 soil, 78 residue). With these two training datasets two classifiers were created. The remaining objects, which were not included in the training data sets, were then classified separately using both classifiers. The probability densities in MLE are assumed to depend on θi, so that $p(X|\omega i, \theta i)$ is the probability of X belonging to class i. For any unknown object with feature vector X, MLE estimated the class that maximized the probability (Duda *et al.* , 2001). To determine the error, the group membership of each object was labelled manually and compared with the classification results.

2.2.2. Results and discussion

The results of the classification based on the first training data set are given in Table 2.1. The overall classification accuracy of correctly classified objects (RUMOB, TAROF, PLAMA , soil and residue) ranged from about 65% to 81% for i=5, whereas for RUMOB vs. residue it was between 71% and 87%, corresponding to between 66 and 121 objects. Detection appeared to be decreasing with time, indicating a change in phenology and morphology creating a change in geometric features.

Finally, the six feature matrices for the six data sets were merged to one feature matrix containing 3861 objects, and then the data were classified again. Overall classification accuracies and RUMOB detection rates of 71% and 78% were determined, respectively. These results are confirmed by the confusion matrix of the classification given in Table 2.2. The largest misclassification rates were for RUMOB and PLAMA, as 125 RUMOB objects (16%) were assigned to PLAMA and in turn 113 PLAMA objects (17%) were assigned to RUMOB. Further misclassifications occurred between the classes residue and soil, with 168 out of 265 soil objects being classified incorrectly as residue. The misclassification rate between TAROF and PLAMA was about 13% and 22%, respectively. Reducing the number of classes to i=2 increased the detection rate considerably (Table 2.1). The overall classification accuracy was on average

Table 2.1.: *Classification results for the classifiers trained with 207 objects from July 19th (RUMOB (R.o.): 45; TAROF: 29, PLAMA: 50; soil: 22; residue: 63)*

Data set	Total number of		Classification into					
			i=5 groups [a]			i=2 groups [b]		
			Detection rate (%)		Total nr. of *R.o.*	Detection rate (%)		Total nr. of *R.o.*
	Objects	*R.o.*	Total	*R.o.*		Total	*R.o.*	
07/19-1	372	82	80.7	80.5	66	90.6	91.5	75
07/19-2	635	128	76.4	86.7	111	90.9	92.2	118
07/22-1	694	142	71.8	75.3	107	90.6	85.9	122
07/22-2	780	146	70.5	82.9	121	87.4	87.7	128
07/28-1	671	157	65.3	73.9	116	88.1	74.5	117
07/28-2	709	127	66.4	70.9	90	89.7	77.9	99
All	3861	782	71.0	78.1	611	89.4	84.3	659

[a] *Rumex obtusifolius* L., *Taraxacum officinale* Web., *Plantago major* L., soil, residue
[b] *Rumex obtusifolius* L. and residue

90%, whereas the rate of RUMOB detected correctly varied from 75% to 92%, again indicating a time dependent decrease. The results of the same classification procedure obtained from the second and independent training set are given in Table 2.3. The total classification rate for the five classes of 67% to 82% was similar to those obtained before, whereas for RUMOB the detection rate increased, ranging from 77% to 92%. For the classification into two groups (RUMOB vs. residue) the overall classification accuracy was similar to that for the July 19th training data set, whereas the RUMOB detection rate increased to 81% and 95%, respectively. As before, all feature matrices were merged (3818 objects) and classified. The corresponding confusion matrix is given in Table 2.2. There was still considerable misclassification for RUMOB and PLAMA (9% and 24%, respectively). Incorrect results for PLAMA and TAROF were 16% and 21%, respectively, and for soil and residue it was 6% and 24%, respectively.

A comparison of Table 2.1 and Table 2.3 shows that the detection rate of RUMOB improved with the classifier trained with data from July 22nd as compared to the July 19th training data set. When the classifier was trained with the data derived on July 19th (Table 2.1),

Table 2.2.: *Confusion matrix indicating misclassifications for the classification of all 3861 objects according to Table 2.1*

			Predicted class					
			Residue	RUMOB	TAROF	PLAMA	Soil	Sum
Original class	Total	Residue	1238	39	122	109	39	1547
		RUMOB	10	611	36	125	0	782
		TAROF	88	19	357	128	1	593
		PLAMA	25	113	86	450	0	674
		Soil	168	8	1	2	86	265
	%	Residue	80.0	2.5	7.9	7.0	2.5	100
		RUMOB	1.3	78.1	4.6	16.0	0.0	100
		TAROF	14.8	3.2	60.2	21.6	0.2	100
		PLAMA	3.7	16.8	12.8	66.8	0.0	100
		Soil	63.4	3.0	0.4	0.8	32.5	100

the accuracy of the classification of the July 28th data was drastically reduced (75% and 78% RUMOB detection rates). In contrast, with the July 22nd training data set, the July 28th data showed much greater rates of detection for RUMOB (81% and 85%). This might have been caused by changes in morphology of the plant leaves during nine days of growth and phenological development which could be even visually observed. The classification results for the detection of RUMOB in mixed grassland swards grown together with similar broad leaved weeds were surprisingly good.

In general, it can be argued that if we fail to identify individual RUMOB plants during classification, it could have serious implications because of the large number of seedlings per plant and its large capacity for germination. Consequently, high detection rates need to be obtained. In this experimental approach, individual plants of RUMOB consisted of more than one isolated object (leaf) in the images. For example, with data set 2 for July 22nd, 121 objects related to RUMOB were detected correctly out of about 60 RUMOB plants in the field, indicating about two objects per plant on average. Consequently, the probability of plant identification must have been greater than the object identification rate of the same individual.

Table 2.3.: *Classification results for the classifiers trained with 252 objects from July 22nd (RUMOB (R.o.): 55; TAROF: 37, PLAMA: 43; soil: 39; residue: 78)*

Data set	Total number of		Classification into					
			i=5 groups [a]			i=2 groups [b]		
			Detection rate (%)		Total nr. of *R.o.*	Detection rate (%)		Total nr. of *R.o.*
	Objects	*R.o.*	Total	*R.o.*		Total	*R.o.*	
07/19-1	581	127	81.8	92.1	117	86.4	91.3	116
07/19-2	635	128	70.6	89.8	115	87.9	95.3	122
07/22-1	442	87	73.3	85.1	74	88.5	90.8	79
07/22-2	780	146	67.2	84.3	123	85.8	92.5	135
07/28-1	671	157	70.2	77.1	121	91.2	80.9	127
07/28-2	709	127	67.3	79.5	101	87.3	85.0	108
All	3818	727	70.6	84.0	611	88.0	89.0	647

[a] *Rumex obtusifolius* L., *Taraxacum officinale* Web., *Plantago major* L., soil, residue
[b] *Rumex obtusifolius* L. and residue

Three main reasons for misclassification were identified. Firstly, there were many errors in the residue class, with residue objects being assigned incorrectly. Such errors could arise from the optical properties of the lens; objects cannot be projected to the image plane without radial symmetric distortions. This effect increases with the distance from the image centre. Hence, the geometry of peripheral weed leaves has been distorted and in addition, peripheral residue objects have been segmented incorrectly. Consequently, derived residue objects varied markedly in colour, texture and shape features. Some of the object features were similar to those of the herb and soil features in the respective training data set, hence causing misclassification. Secondly, greater misclassification of RUMOB occurred at later growth stages, indicating that differences in colour, texture and shape of RUMOB leaves increased with plant age. Thirdly, RUMOB and PLAMA objects were assigned incorrectly to their respective classes because their features were unexpectedly similar. Clearly, the identification features of the two plant species used so far are not sufficiently typical for either class.

Table 2.4.: *Confusion matrix indicating misclassifications for the classification of all 3818 objects according to Table 2.3*

			Predicted class					
			Residue	RUMOB	TAROF	PLAMA	Soil	Sum
Original class	Total	Residue	1135	10	111	186	90	1532
		RUMOB	5	651	44	72	0	772
		TAROF	86	14	350	125	10	585
		PLAMA	12	161	106	399	3	681
		Soil	59	1	2	2	184	248
	%	Residue	74.1	0.7	7.2	12.1	5.9	100
		RUMOB	0.6	84.3	5.7	9.3	0.0	100
		TAROF	14.7	2.4	59.8	21.4	1.7	100
		PLAMA	1.8	23.6	15.6	58.6	0.4	100
		Soil	23.8	0.4	0.8	0.8	74.2	100

2.3. Impact of feature combinations

2.3.1. Materials and methods

It was tested how single features of geometry, colour and texture influenced the classification results. Therefore, seven new training data sets were derived from the data recorded on July 22nd each comprising the following features and combination of features (see also chapter 2.2.1.2).

1. means of ∇f
2. means of I, G and R
3. *Eccentricity*, *Circularity* and *Shape Factor*
4. *Area*, *Perimeter*, *Eccentricity*, *Circularity* and *Shape Factor*
5. means of ∇f and means of I, G and R
6. means of ∇f, means of I, G, R, *Eccentricity*, *Circularity* and *Shape Factor*

7. all features

Based on these training data sets, seven separate classifications were computed with the six feature matrices recorded on the three dates of image acquisition, plus one feature matrix that originated from merging the six entire feature matrices. The detection rates were stored in 7 × 7 matrices according to the seven training data sets and the seven classified feature matrices. As a result, four such matrices were derived, two matrices each for overall classification accuracies or RUMOB detection rates both for the classification into either i=5 or i=2 classes.

A rank analysis was done on these four matrices to identify the training data set that performed best. As there were seven classifiers to be compared, the ranks ranged from one to seven. The classification with the highest detection rate was ranked one. The mean rank for all seven classifications was calculated for each of the four matrices, then the means of the ranks were summed. The classifier with the smallest sum of means was considered to be the best.

2.3.2. Results

The rank analysis of the experimental data was used to identify those features of the object and their combinations that provided the best classification results. The average ranks for i=5 and i=2 of the total and RUMOB specific detection rates are given in Table 2.5. The final column indicates the sum of these ranks. The lowest ranks indicate the best classification results for all classifications on average. Separately applied geometric, colour or textural features resulted in the highest ranks and therefore the poorest classifications. For example, the classification into i=5 groups using only geometry features (training data sets 2-4) resulted in overall classification accuracies ranging from 40% to 60%. When using texture features exclusively, the detection rate was between 60% and 70%. Merging gradient and colour features (training data set 5) increased the overall classification accuracy (65%- 82%). This training dataset led to the third best classification results in this analysis with a sum of average ranks of 10.4. The best results were obtained by combining all features (training dataset 7). In general, the overall classification accuracies of the three best ranked training data sets varied less than about 5%, but in particular cases the differences were between 10% and 20%.

Table 2.5.: *The average ranks of the detection rates for the classifications of 7 data sets based on training data sets with different features*

Training data set (feature combination)	Average ranks of detection rates of				Sum of ranks
	i=5 [a] classification		i=2 [b] classification		
	Total	RUMOB	Total	RUMOB	
1 ($\mu_{\nabla f}$)	4.0	3.6	2.3	3.3	13.2
2 (μ_I, μ_R, μ_G)	5.7	4.9	6.4	5.3	22.3
3 (*Eccentricity*, *Circularity*, *ShapeFactor*)	5.3	6.4	6.0	6.6	24.3
4 (*Eccentricity*, *Circularity*, *ShapeFactor*, *Area*, *Perimeter*)	7.0	5.7	4.9	5.6	23.2
5 ($\mu_{\nabla f}$, μ_I, μ_R, μ_G)	1.6	3.6	1.6	3.6	10.4
6 ($\mu_{\nabla f}$, μ_I, μ_R, μ_G, *Eccentricity*, *Circularity*, *ShapeFactor*)	2.7	1.9	3.0	2.1	9.7
7 (All features)	1.6	1.4	3.4	1.7	8.1

[a] *Rumex obtusifolius* L., *Taraxacum officinale* Web., *Plantago major* L., soil, residue
[b] *Rumex obtusifolius* L. and residue

3. Improved image classification algorithm for automatic *Rumex obtusifolius* detection using colour and texture object features

3.1. Introduction

In chapter 2 an approach for the automatic detection of RUMOB in grassland swards versus PLAMA and TAROF by digital image processing is described. Colour images were used taken at close-range from experimental plots planted with different weed species at different stages of growth. An object-oriented image classification was done on these images using local homogeneity (Cheng & Sun, 2000) and image morphology for image segmentation. The remaining objects were classified using a Maximum Likelihood Estimation into five groups: (i) RUMOB, (ii) TAROF, (iii) PLAMA, (iv) soil (gaps), and (v) a residue class. Nine features were calculated to describe the shape, colour and texture of each object.

High detection rates of RUMOB were achieved. However, the overall classification accuracy was rather low, because of high misclassification in the residue class,a non-acceptable high misclassification of PLAMA with RUMOB and a decrease of classification accuracy at later growth stages. The study also exhibited a strong contribution of colour and texture features to the discrimination between weed species, even if highest accuracy was achieved when combining them with geometrical object features.

With these results and conclusions the classification procedure was modified to answer the following questions:

(1) Is it possible to increase the accuracy of 71% to 92% for RUMOB classification by calculating more textural and colour features?;

(2) Can the large rates of misclassification of PLAMA be reduced in this context?

3.2. Materials and methods

3.2.1. Modified image processing

This analysis was conducted on the same 108 images as in the previous investigation. All images were segmented using the same procedure described above. First, the 24-bit red-green-blue (RGB) images were transformed to 8-bit intensity images (I). The standard deviation image, S, and the gradient image, ∇f, were both calculated based on I. The local homogeneity image H (Cheng & Sun, 2000) was calculated as $H = 1 - \nabla f_{ij}/\nabla f_{ij_{max}} \bullet S_{ij}/S_{ij_{max}}$, where ${}_{ij}/S_{ij_{max}}$ and $\nabla f_{ij}/\nabla f_{ij_{max}}$ are the maximum normalized standard deviation image and gradient image, respectively. By applying an empirical threshold, TS, of 0.97 to the local homogeneity image leaf regions were separated successfully. The remaining regions in the resulting binary image were not only weed leaves but also blades of grass, which pixels were connected to the weed pixels in the images and formed contiguous regions. Therefore, morphological opening was applied to the binary image with a diamond Structure Element (SE) with a radius of three pixels. Finally, all image regions smaller than 5000 pixels (equivalent to 17 cm^2 in nature) were eliminated. The remaining contiguous image regions, further called objects, were RUMOB, PLAMA, TAROF, soil, or a residue class.

3.2.2. Feature extraction and feature evaluation

The aim of the analysis is to classify the objects derived by image segmentation into a defined number of classes according to their specific features. In the previous investigation geometrical features (*Area*, *Perimeter*, *Eccentricity*, *Roundness*, *ShapeFactor*), colour features (means of the intensity, the red and the green object pixels) and one texture feature (mean of the gradient object pixels) were calculated for each object. The best classification results were achieved when all features were included in classification. The texture feature contributed most to the classification result and when used in combination with the colour features resulted in classi-

fication rates close to those obtained using all nine features. In this investigation additional colour and texture features were included resulting in 17 object features (Table 3.1).

Table 3.1.: *The calculated object features. μ is the mean and σ is the standard deviation derived from the object pixels in the red image channel (R), the green image channel (G), the intensity image (I), the standard deviation image (S), the gradient image (∇f) and the local homogeneity image (H)*

Total number		
Geometry	Colour	Texture
V1. *Area*	V6. μ_R	V12. μ_S
V2. *Perimenter*	V7. μ_G	V13. $\mu_{\nabla f}$
V3. *Eccentricity*	V8. μ_I	V14. μ_H
V4. *Roundness*	V9. σ_R	V15. σ_S
V5. *ShapeFactor*	V10. σ_G	V16. $\sigma_{\nabla f}$
	V11. σ_I	V17. σ_H

To determine which features contribute most to the classification, a stepwise discriminant analysis was performed using Statistical Product and Service Solutions (SPSS) 12.0 software (© SPSS Inc.) on the 17 object features for the 694 objects derived from the first 18 images of July 22nd. The group membership for each of the 694 objects was labelled manually and Wilks's lambda was used to test the significance of the discriminant functions. Wilks's lambda (Λ) is a test statistic used in Multivariate ANalysis Of VAriance (MANOVA) to test whether there are differences between the means of more than two identified groups of subjects on a combination of dependent variables. In stepwise discriminant function analysis, a model of discrimination is built step-by-step. Specifically, at each step all variables are reviewed and evaluated to determine which one will contribute most to the discrimination between groups, which is the variable that minimizes the overall Wilks' Lambda. That variable will then be included in the model, and the process starts again.

3.2.3. Classification

A Maximum Likelihood classification was used to group the image objects into the five classes: (i) RUMOB, (ii) TAROF, (iii) PLAMA, (iv) soil, and (v) residue. The MATLAB (© The

Table 3.2.: *The variables (features) remaining after stepwise discriminant analysis and Wilks's Lambda*

Step	Entered Variables	Wilks'Lambda
1	V14	0.209
2	V7	0.150
3	V8	0.092
4	V17	0.079
5	V15	0.070
6	V12	0.046
7	V16	0.040
8	V13	0.038
9	V11	0.036
10	V6	0.034
11	V1	0.032
12	V9	0.031
13	V10	0.029

MathWorks, Inc.) Classification ToolBox (Stork *et al.* , 2004) was used for this purpose. A classifier was created with those features (variables) that were not removed by discriminant analysis. It was trained with the feature vectors of the 694 objects segmented in the first 18 images from July 22nd. The remaining objects not included in training (1261 for July 19th, 780 for July 22nd, 1380 for July 28th) were then classified. Group membership of each object was labelled manually and compared to the classification results. Total classification accuracy, RUMOB detection rates and percentage of objects misclassified as RUMOB were calculated. The classification results were stored in confusion matrices to assess the error. The results were compared to those of the classifier described in chapter 2.

3.3. Results and discussion

3.3.1. Feature evaluation

In the images of the 19th, 22nd, and 28th of July, 1261, 1474, and 1380 objects were segmented, respectively. The 694 objects from the first 18 images of July 22nd were used in

Table 3.3.: *Confusion matrix indicating classification accuracies (%) and misclassifications (%) for the classifications of image objects from July, 19th , 22nd and 28th into the defined classes of Rumex obtusifolius (RUMOB), Taraxacum officinale (TAROF), Plantago major (PLAMA), soil and residue*

Data set	%			Predicted class				
				Residue	RUMOB	TAROF	PLAMA	Soil
July, 19th	82.7	Original	Residue	86.0	0.8	8.7	0.4	4.1
		class	RUMOB	0.0	91.4	3.9	4.7	0.0
			TAROF	11.9	4.0	74.4	8.0	1.7
			PLAMA	6.8	6.8	16.2	70.3	0.0
			Soil	10.6	0.0	0.0	0.0	89.4
July, 22nd	80.4	Original	Residue	78.2	0.9	11.8	3.3	5.8
		class	RUMOB	0.0	92.5	6.2	1.4	0.0
			TAROF	15.2	2.0	72.7	9.1	1.0
			PLAMA	2.9	1.4	17.4	76.8	1.4
			Soil	16.4	0.0	0.0	0.0	83.6
July, 28th	75.9	Original	Residue	81.5	1.2	9.6	2.0	5.7
		class	RUMOB	1.8	85.2	9.2	3.5	0.4
			TAROF	20.1	6.7	61.9	11.3	0.0
			PLAMA	7.5	3.4	20.7	68.0	0.4
			Soil	24.4	0.0	0.0	0.0	75.6

stepwise discriminant analysis, and 13 of the 17 features (variables) were considered to contribute significantly to discrimination (Table 3.2). The mean local homogeneity of the objects (V14) had the most influence on discrimination. The means of green (V7) and intensity object pixels (V8) were rated second and third, followed by the remaining texture and colour features. The four features excluded were features V2-V5, which are the geometric measures. Feature V1, area, led to calculation errors when training the classifiers and so this feature was also excluded. For further analysis only the 12 features related to colour and texture were used.

Table 3.4.: *The improved classification results for the new classification algorithm (C2) as compared to the algorithm (C1) from Experiment 1*

Classifier	Data	Total detection rate [%]	RUMOB detection rate [%]	TAROF to RUMOB error [%]	PLAMA to RUMOB error [%]	SOIL to RUMOB error [%]	Residue to RUMOB error [%]
C1	07/19	75.4	84.7	2.8	15.8	0.0	0.0
	07/22	70.0	78.8	2.0	18.8	0.0	0.0
	07/28	69.7	71.5	1.7	9.0	0.0	0.2
C2	07/19	82.7	91.4	4.0	6.8	0.0	0.8
	07/22	80.4	92.5	2.0	1.4	0.0	0.9
	07/28	75.9	85.2	6.7	3.4	0.0	1.2

3.3.2. Classification results

The overall classification accuracy for all the images of July 19th was 82.7%, for July 22nd, 80.4% and for July 28th, 75.9%. The confusion matrices in Table 3.3 show the trends of misclassification for each of the three sets of data that were classified. Most misclassifications of RUMOB objects were again with PLAMA and TAROF. However, compared to the results of chapter 2, the detection rates in the analysis increased dramatically (Table 3.4). With the classifier of chapter 2 the overall classification accuracy ranged from 69.7% to 75.4%, whereas with the new classifier accuracies of between 75.9% and 82.7% were achieved. Likewise, the RUMOB classification accuracy increased to between 85.2% and 92.5%, whereas before it ranged from 71.5% to 84.7%. Moreover, the misclassification between RUMOB and PLAMA was reduced: only 1.4% to 4.7% of RUMOB objects were classified wrongly as PLAMA, and 1.4% - 6.8% PLAMA objects were classified wrongly as RUMOB (Table 3.3). Furthermore, there was misclassification with RUMOB vs. TAROF with 2.0% to 6.7% of TAROF objects being classified wrongly as RUMOB.

It is hardly possible to value these results in the context to the so far published investigations on weed species discrimination in arable crops for the reasons mentioned before. However, even there the reported classification rates vary from moderate to excellent. For example Petry and Kühbauch (Petry & Kühbauch, 1989) discriminated between six weed species seedlings using

shape parameters with an average accuracy of 82.3%. Meyer *et al.* (Meyer *et al.* , 1998) discriminated two species of grasses from two broadleaf weed species by Colour Co-occurrence Method (CCM) with classification accuracies of 93% and 85%, respectively. Classification accuracies of the individual species only ranged from 30% to 77%. Burks *et al.* (Burks *et al.* , 2000) also used CCM and classified between five weed species and soil with an accuracy of 93%. In our investigation, overall accuracy of discriminating three grassland weed species, soil, and residue did not exceed 83%. Still taking into account that our main focus was on detecting RUMOB the rate was up to very high 93% as related to individual leaf objects. Since the average RUMOB plant may consist of more than one leaf (see chapter 2.2.2 the rate of plant identification must have been greater than the object identification rate.

4. The influence of image spatial resolution on the classification accuracy

4.1. Introduction

One major constraint in most published investigations on image classification algorithms for weed discrimination is the lack of information about processing time. Besides the high resolution required for discriminating weed species individuals, ground-based sensing theoretically offers the possibility to be implemented in on-line solutions for site-specific weed management. Those systems, however, are only viable when the processing time of images is rather fast. Therefore, besides the focus on highest classification accuracies, studies should also concentrate on classification performance in terms of processing time. So far, there are only few studies reporting about real-time solutions. *E.g.* Marchant *et al.* (1998) developed an image processing system for real-time segmentation of plant and weeds in arable crops. With that, weed species discrimination is not possible. Gerhards and Oebel (2006) recently reported about practical experiences with real-time image analysis and weed spraying. The image processing, however, was performed off-line and hence the system so far requires at least three steps, image collection, image processing and herbicide application.

The time needed for classifying images is mainly defined by the size of the images. Especially in the image segmentation, where filters or morphological operations are often applied, most time is used. The only solution for speeding up the classification is to decrease the size of the images. This requires the knowledge about the influence of the image resolution on the classification accuracies. In this experiment the images used for algorithm development have been decreased in six steps, giving pixel sizes ranging from 0.6 up to 3.0 mm. Typical resolutions

available with commercial industrial cameras have been chosen. The smallest resolution available with most camera distributors is 480 × 640. This resolution has therefore been chosen to be the smallest in this investigation. The image segmentation was adjusted to the lower resolutions. For each image resolution, classifiers were created by training with test samples, as in the studies before. Classification accuracies and processing time was monitored for each of the image classifications.

4.2. Materials and methods

The pixels of the same 108 images as in the previous studies were aggregated progressively to give six different resolutions (Table 4.1). The MATLAB *imresize* function with nearest-neighbour interpolation was used to resize the images. The resolutions of the images ranged from 2448 × 3246 pixels to 480 × 640 pixels. The resulting images were segmented using a modified version of the procedure described above. As a result of the change of scale in the upscaled images, the area threshold and size of structure element for morphological opening were adjusted to the image resolution (Table 4.1). In addition, the grey-level threshold applied to the local homogeneity image for generating binary images was calculated dynamically for each image as $TS = \mu_H$, which is the mean of the local homogeneity over the whole image. This TS is not static as in chapter 2.2.1.1 and is adjusted to the gradient distribution of every individual image automatically.

Table 4.1.: *The image resolutions and changing parameters in image segmentation*

Image resolution	Pixel size [mm]	Area threshold [pixels]	Size of structure element [pixels]
2448 × 3264	0.6	5000	8
1704 × 2272	0.7	2450	7
1200 × 1600	1.2	1220	6
1024 × 1280	1.5	610	5
768 × 1024	1.9	480	4
480 × 640	3.0	190	3

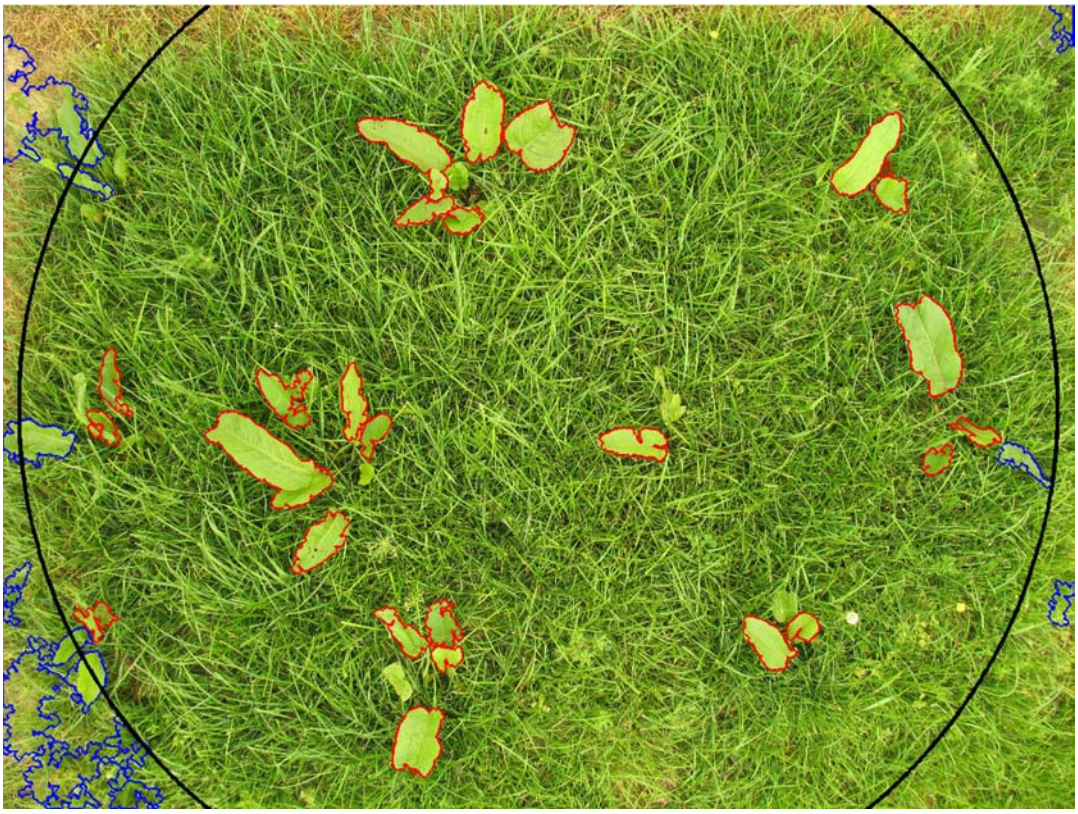

Figure 4.1.: *Confidence circle CC: only the red objects lying completely within the black circle are included in the classification*

With the previous experiments it could be shown that image distortion led to over-segmentation at the image borders and to misclassification. Therefore, in this chapter a confidence circle, (CC) was defined with a diameter of 97% of the image x-dimension (Eq. (4.1)) and with its origin at the image centre. Only those image objects that were completely contained by the confidence circle were included in further analyses (Figure 4.1).

$$CC : (x - \frac{x_{dim}}{2})^2 + (y - \frac{y_{dim}}{2})^2 = (\frac{0.92 \bullet x_{dim}}{2})^2 \tag{4.1}$$

As in chapter 3, the 12 features retained by the discriminant analysis were calculated for those confident image objects. Maximum Likelihood classification was then applied to these data. Four classes were defined: (i) RUMOB, (ii) PLAMA, (iii) TAROF + residue and (iv) soil. Because of the small number of residue objects resulting from segmentation at the three higher image resolutions (see Fig. 4.2) it was not sensible to establish a standalone class and

so they were combined with the TAROF class. Both, TAROF and residue classes are tolerable entities in grassland. The objects for the six image resolutions were classified separately. Three training data sets (T1-T3; all image objects from the first 18 images of July 19th, July 22nd and July 28th, respectively) were derived for each of these six data sets. The remaining objects not included in the training data set were then classified. We had three different training datasets for each of the six image resolutions and three datasets to be classified. Hence, in total we performed 54 independent classifications.

The result of each of these classifications was represented by a single value, the quality index (QI). This single measure enables all of the classification results to be compared rather than using separate measures such as classification accuracies, detection rates for each species (group) and the respective misclassifications to RUMOB. This index was designed specifically for the evaluation of this investigation and might not be suitably applied to other studies. It provides a measure for the quality of a RUMOB distribution map, which can be used to guide a herbicide sprayer. The RUMOB detection rate should be as large as possible to avoid missing such plants when spraying. On the other hand, the rate of objects classified wrongly as *Rumex obtusifolius* L. should be as small as possible, because they appear as RUMOB in the map and then would be sprayed wrongly in practice. The quality index QI (Eq. (4.2)) was derived from the RUMOB classification accuracy (R) (Eq. (4.3)) and the weighted misclassifications (E_w) of other objects to RUMOB.

$$QI = 1 - R + E_w \tag{4.2}$$

$$R = \frac{C_{RUMOB}}{N_{RUMOB}} \tag{4.3}$$

where C_{RUMOB} is the number of RUMOB objects classified correctly and N_{RUMOB} is the total number of RUMOB objects. The classification accuracy, R, was calculated as an independent summand in Eq. (4.3). It is not weighted by the total number of objects because every RUMOB object has to be detected independently from the total number of objects to be classified. The value of R ranges from 0 to 1; the maximum is where all RUMOB objects have been classified correctly. The error (E) of objects classified wrongly as RUMOB for the i=3 non-RUMOB groups x_i [$i \in$(PLAMA;TAROF/Residue;Soil)] is calculated with Eq. (4.4).

$$E = \sum_{i=1}^{3} \frac{Ex_i}{Nx_i} \tag{4.4}$$

Ex_i and Nx_i are the number of objects wrongly classified as RUMOB and the total number of objects within the groups x_i, respectively. This error is overestimated if the number of objects in the classes, x_i, is small compared to the number of RUMOB objects. Therefore, each of the misclassification rates, Ex_i, was weighted by the total number of objects to be classified (N_{TOTAL}) (Eq. (4.5)).

$$E_w = \sum_{i=1}^{3} \frac{Ex_i}{Nx_i} \bullet \frac{Nx_i}{N_{TOTAL}} = \sum_{i=1}^{3} \frac{Ex_i}{N_{TOTAL}} \tag{4.5}$$

The quality index, QI, ranges from zero to two; it decreases towards to zero for all non-RUMOB objects misclassified as RUMOB and all RUMOB objects that are misclassified. The value would be close to one if all non-RUMOB objects are classified as RUMOB and all RUMOB objects are classified correctly. Values close to two indicate low misclassification and high RUMOB classification rates.

The QI was calculated for each of the above-mentioned classifications and values were stored into a 6×9 matrix. These values were summed up for each image resolution. The largest summed values indicated the image resolution most suitable for RUMOB detection.

The time taken for the segmentation and feature extraction of the 36 images from July 22nd was documented for each of the six image resolutions. The number of objects per image did not exceed 50, therefore this number was chosen to test the classification performance. The classification of 50 randomly selected objects was performed 100 times and the elapsed time was documented. The mean of the elapsed time was considered to be the maximum for processing the classification of image objects. The time needed for image acquisition was not analysed because the images did not come directly from the camera but were stored to compact flash card before transfer to the computer. The analysis was done with MATLAB desktop. The operating system was Windows XP/2002 Professional. The processor was a Intel Pentium 4 with 1.60 GHz CPU and a working memory of 1024 MB DDR-SDRAM.

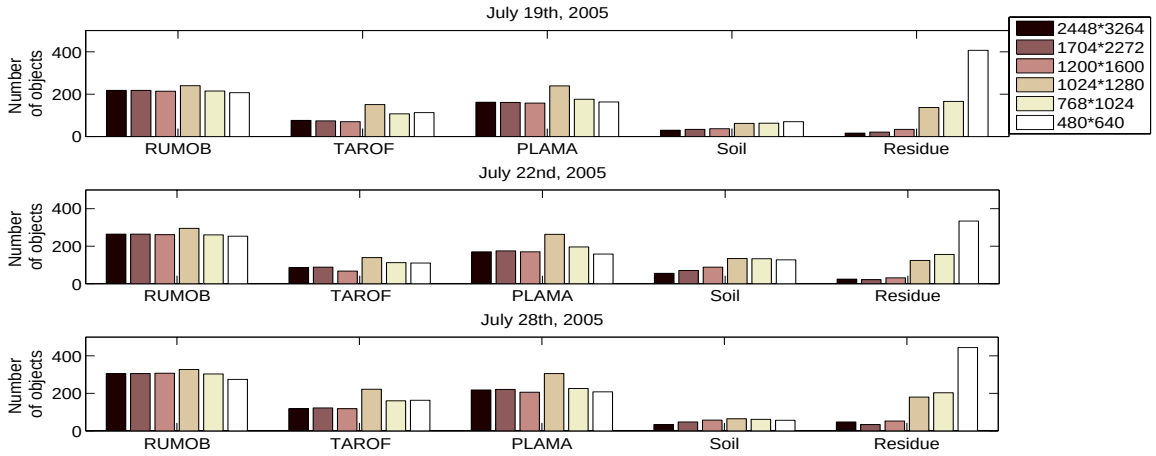

Figure 4.2.: *Number of segmented objects at different image resolutions*

4.3. Results and discussion

The change of image resolution resulted in a change in the number of segmented objects for each of the resolutions. Figure 4.2 shows that the number of segmented weeds is comparable to some extent for all six resolutions. There was a small increase in the number of segmented objects for the soil class as the image resolution decreases from a maximum of 1024 × 1280 pixels to the lower resolutions. There was more than a 10-fold increase in the number of residual objects at the lowest image resolution compared with the highest one. This increase was caused by over segmentation of the low-resolution images (Figure 4.3). In other words, objects were derived that did not actually represent homogeneous image regions, for example as weed leaves or soil. Obviously, the chosen resampling method for generating the different resolutions led to image artefacts, which were the regions segmented wrongly.

For each of the six image resolutions (Table 4.1) three training data sets and hence three classifiers were established with the objects from the first 18 images of July 19th, 22nd and 28th. The image objects not included in training of all data sets were then classified. The classification and error rates for the six image resolutions are given in Table 4.2. Classification accuracy ranged from 65.2% to 86.2%. The lowest rates were for image resolutions of 1024 × 1280 pixels and 768 × 1024 pixels (65.2% - 76.1% and 67.1% - 78.2%, respectively). For the other resolutions classification accuracies of up to 86% were achieved. Comparing these results

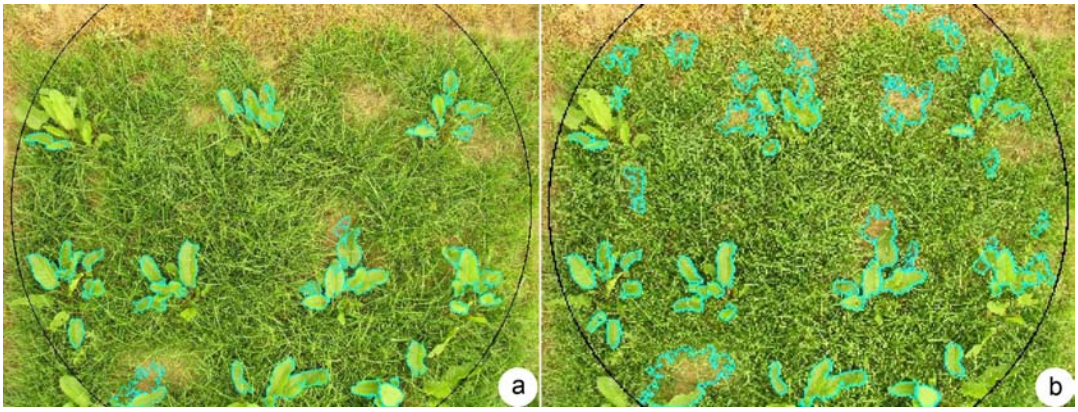

Figure 4.3.: *The increase in over-segmentation with reduced image resolution: (a) segmented objects at a resolution of 2448 × 3264 pixels and (b) segmented objects at a resolution of 480 × 640 pixels*

to those in Figure 4.4 for all classifications, it is evident that the lower rates of classification and RUMOB detection were for classifying data from July 28th or when training the classifier using the July 28th data. The plants showed advanced stages of growth by this date and there was an increase in the overlap between weed leaves and grasses. Table 4.2 supports these observations with the classification rates errors for RUMOB. The classification accuracy for RUMOB is up to 94.7% (Table 4.2). The smallest percentage accuracies are for resolutions 1024 × 1280 pixels and 768 × 1024 pixels (63.0% and 57.1%, respectively). These smallest detection rates are for the classification of July 28th data using classifiers trained with data from July 19th or 22nd (Figure 4.4). In general, the errors for PLAMA and TAROF/Res. are <10%. Errors >10% are for the July 28th data. There was generally no misclassification of soil. When applying a classificator of one resolution, *e.g.* 2448 × 3264, to images with differing resolution the classification accuracy was worse. Actually, the selected object features tend to be scale independent, since they use the local object histograms only. However, training data sets derived for one resolution apparently do not represent objects at other image resolutions sufficiently. This might be caused by the applied nearest-neighbour interpolation resulting in artefacts as a result of Aliasing.

The quality indices (QI) are given in Table 4.3. The indices for all image resolutions were summed and then ranked. The largest sum of quality indices has been found with an image resolution of 1704 × 2272 pixels, followed by image resolutions 2448 × 3264, 480 × 640 and

Table 4.2.: *Classification results derived from images with different resolutions*

Image resolution	Total detection rate [%]	RUMOB detection rate [%]	TAROF/Res. to RUMOB error [%]	PLAMA to RUMOB error [%]	SOIL to RUMOB error [%]
2448 × 3264	72.4-83.8	78.5-94.7	2.6-19.7	3.3-12.4	0.0-3-0
1704 × 2272	68.5-86.2	80.3-94.5	3.0-21.6	0.0-8.2	0.0
1200 × 1600	68.5-82.5	72.0-92.1	3.2-17.8	2.7-10.4	0.0
1024 × 1280	65.2-76.1	63.0-84.4	0.0-11.9	2.1-13.7	0.0
768 × 1024	67.1-78.2	57.1-91.2	3.1-12.1	4.4-17.0	0.0
480 × 640	72.4-80.4	81.8-91.4	1.8-9.7	4.3-17.5	0.0-1.4

1200 × 1600 pixels. As indicated in Table 4.2 the image resolutions 1024 × 1280 pixels and 768 × 1024 pixels rank the lowest because they had the lowest RUMOB detection rates. Table 4.4 shows the elapsed time for the image processing steps. For the full resolution images up to 45 seconds were needed for processing. Reducing the image resolution to 480 × 640 pixels decreased the processing time considerably to 2.5 seconds on average.

Table 4.3.: *Quality indices for the classification with different training data sets and the different image resolutions (Img. res.): (a) 2448×3264; (b) 1704×2272; (c) 1200×1600; (d) 1024×1280; (e) 768×1024; (f) 480×640.*

Img.	RUMOB quality index for classification with:									Sum	Rank
res.	T1: Training July 19th			T2: Training July 22nd			T3: Training July 28th				
	Classified data set										
	19th	22nd	28th	19th	22nd	28th	19th	22nd	28th		
a	1.92	1.92	1.78	1.78	1.89	1.78	1.77	1.89	1.75	16.48	2
b	1.90	1.91	1.76	1.91	1.93	1.80	1.89	1.90	1.86	16.85	1
c	1.72	1.83	1.70	1.88	1.89	1.70	1.83	1.80	1.84	16.20	4
d	1.77	1.78	1.61	1.72	1.79	1.69	1.78	1.75	1.78	15.69	6
e	1.73	1.85	1.77	1.76	1.80	1.55	1.81	1.78	1.78	15.82	5
f	1.83	1.79	1.79	1.84	1.79	1.79	1.87	1.80	1.87	16.35	3

Table 4.4.: *Elapsed time in seconds for image segmentation, feature extraction and classification separated by image resolution*

Processing step	Image resolution					
	2448 × 3264	1704 × 2272	1200 × 1600	1024 × 1280	768 × 1024	480 × 640
Image segmentation and feature extraction	42.7013	21.4804	11.0549	9.9453	5.7607	2.4536
Classification	≤ 0.0362					

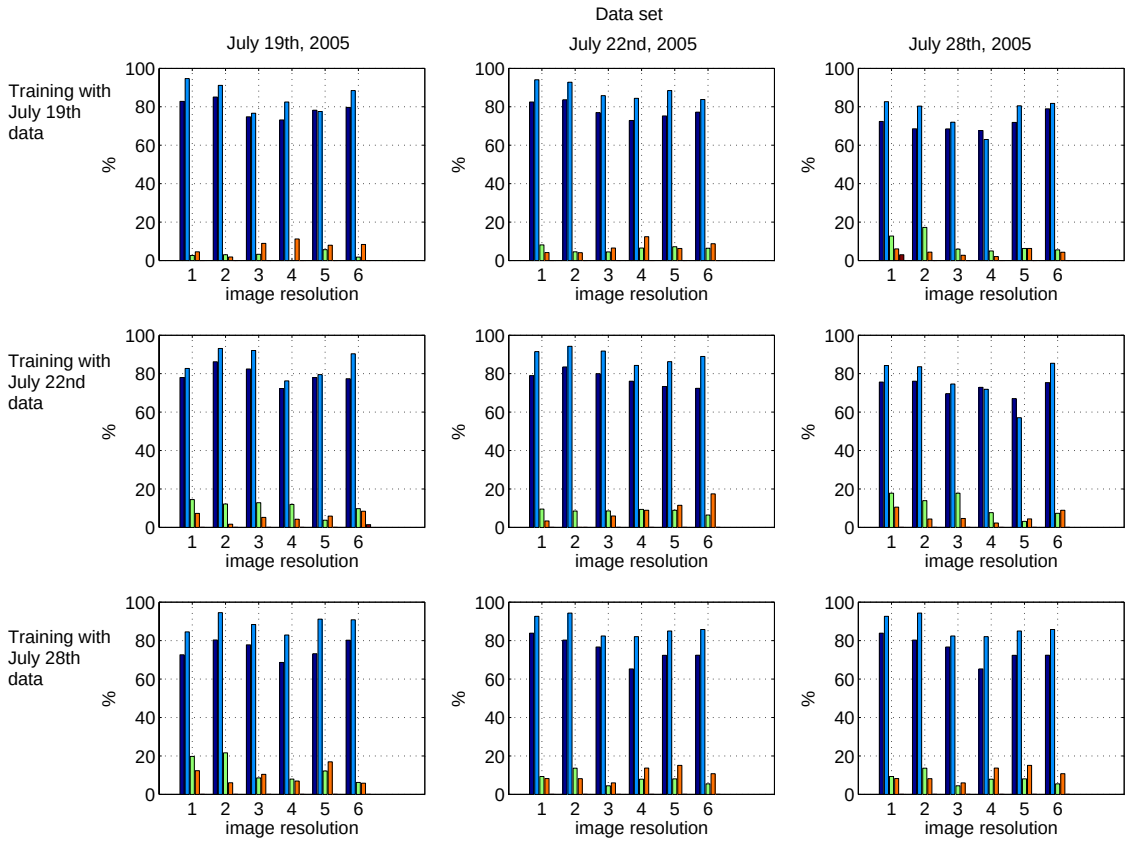

Figure 4.4.: *Classification results for the 54 classifications which comprised six image resolutions: (1) 2448 × 3264, (2) 1704 × 2272, (3) 1200 × 1600, (4) 1024 × 1280, (5) 768 × 1024, (6) 480 × 640, for three training datasets each (the objects from the first 18 images of July 19th, 22nd and 28th data), and three data sets to be classified comprising the remaining objects from July 19th, 22nd and 28th that were not included in training. Dark blue: the overall classification accuracy; light blue: the RUMOB detection rate; green: rate of TAROF and residue misclassified as RUMOB; orange: rate of PLAMA misclassified as RUMOB; brown: rate of soil misclassified as RUMOB*

5. Mapping *Rumex obtusifolius* during different grassland growths based on automatic image classification and GIS

5.1. Introduction

The date of application of site-specific weed control is limited by two requirements: (1) the target weeds must be at a growth stage perfectly suited for being detected by the image classification algorithm. In arable crops for example, where some algorithms focus on weed discrimination using leaf shape properties (Franz *et al.* , 1991a; Gerhards *et al.* , 2002; Neto *et al.* , 2006) this is when the weeds are in the seedling stage. However, with starting leaf overlapping and increasing crop cover, weed discrimination is becoming difficult; (2) the application of herbicides must take place when best effectiveness of the chemicals can be achieved. This is defined by the phenological stage of plants, temperatures or even moisture. The best weed detection system is the one who brings both dates together. And keeping in mind the on-line solution this is another fundamental requirement.

In contrast to arable crops, grasslands in Central Europe can be harvested up to three or even four times the year. Thus, there are multiple grassland growths on which the automatic RUMOB detection and chemical controlling could be theoretically applied. The best herbicide efficiency in RUMOB is defined by the phenological stage and the weather conditions. Most herbicides against RUMOB shall be applied in the late summer, when the rosette is fully established but before plants start to flower (Kessler & Ammon, 1996; Zwerger & Ammon, 1999).

The present complementary study focuses on the multi-temporal mapping of RUMOB using

the same procedure of image processing with the images taken at 13 dates over the spring growth and the regrowth of grass plots in 2006, as in the year before. The aim was not to derive classification accuracies of the image classification algorithm again but to translate the results of image classification into application maps for site-specific spraying. The resulting herbicide application maps were compared to the reality in the experimental plots. Best results were figured and compared to herbicide instruction manuals.

5.2. Materials and methods

5.2.1. Image acquisition and classification

The field experiment was extended in late 2005 to give a total of 54 grassland plots (compare Chapter 1.5). Images were taken using the automated acquisition technology at 13 dates during two grassland growths in 2006. In the spring growth, images were taken at May 23rd and 29th, June 14th, 20th, and 26th and July 5th. The second growth of the grass plots was covered by images taken on July 11th, 20th, and 31st, August 15th and 29th, and September 8th and 12th. In total of 702 images were acquired.

The automatic procedure of image processing and classification applied to the images is described in chapters 2 - 4. According to the results in chapter 4 all images were resized to 480 $\times$ 640 pixels. For the purpose of automatic image classification a software tool was developed within MATLAB (© Mathworks, Inc.) which allows the batch processing of all 54 images per recording date. The result is a list of 54 vectors with the image coordinates and areas of all RUMOB objects per image as well as a report of the classification results for each image as Microsoft Excel© data sheet.

5.2.2. Mapping of RUMOB distribution and the derivation of herbicide application maps

The aim of the subsequent processing steps was to transform the image coordinates of all objects classified as RUMOB into the Gauss-Krueger coordinate system which is the official topographic coordinate system in Germany. The image coordinates for the objects are calculated as the centroid from the object boundaries. With that, for an image with n objects a

coordinate vector $\overline{x}_{IMG}$ with n coordinate pairs is available.

$$\overline{x}_{IMG} = \begin{bmatrix} \overline{x}_{IMG_i} \\ \overline{y}_{IMG_i} \end{bmatrix}_{i=1}^{n} = \begin{bmatrix} x_{IMG_1} & \dots & x_{IMG_n} \\ y_{IMG_1} & \dots & y_{IMG_n} \end{bmatrix}$$

In total, for each recording date 54 coordinate lists were available for 54 images. The object coordinates of each image were transformed into the respective experimental plots. The centroid coordinates $\overline{x}_{Centroid}$ for each of the 54 experimental plots were derived by GPS survey. Per definition, the point of origin (O_{IMG}) in the image coordinate system is the upper left image corner. However, the reference point in the respective plot is the centroid. Therefore, the new point of origin (O'), which is the image centre, was derived by Eq. (5.1), where $x_{IMG_{max}}$ and $y_{IMG_{max}}$ are the image dimensions in x (640 pixels) and y (480 pixels) direction, respectively. The new object image coordinates $\overline{x'}_{IMG}$ were then calculated according to O' using Eq. (5.2).

$$O' = \begin{bmatrix} O'_x \\ O'_y \end{bmatrix} = \begin{bmatrix} \frac{x_{IMG_{max}}}{2} \\ \frac{y_{IMG_{max}}}{2} \end{bmatrix} \tag{5.1}$$

$$\overline{x'}_{IMG} \begin{bmatrix} x'_{IMG_i} \\ y'_{IMG_i} \end{bmatrix}_{i=1}^{n} = \begin{bmatrix} x_{IMG_i} - O'_x \\ O'_y - y_{IMG_i} \end{bmatrix}_{i=1}^{n} \tag{5.2}$$

After resizing the images to 480 × 640 pixels, the size of a pixel in the image center is around 3 mm. By multiplying these new coordinates with the spatial pixel size (PS) of 0.003 m the image coordinates were transformed to the metric system (Eq. (5.3)). In doing so, we simply assumed that the image distortions, which increase towards to the image border, can be neglected.

$$\overline{x}_{METRIC} = \overline{x'}_{IMG} \bullet PS = \begin{bmatrix} x'_{IMG_i} \\ y'_{IMG_i} \end{bmatrix}_{i=1}^{n} \bullet PS \tag{5.3}$$

By applying an affine transformation (Eq. (5.4)) to $\overline{x}_{METRIC}$ the object coordinates were finally transformed into Gauss-Krueger system.

$$\overline{x}_{GK} = A^T \bullet \overline{x}_{METRIC} = \begin{bmatrix} cos(\alpha) & -sin(\alpha) & 0 \\ sin(\alpha) & cos(\alpha) & 0 \\ P_{GK_x} & P_{GK_y} & 0 \end{bmatrix}^T \bullet \begin{bmatrix} x_{METRIC_1} & ... & x_{METRIC_n} \\ y_{METRIC_1} & ... & x_{METRIC_n} \\ 1 & ... & 1 \end{bmatrix} \quad (5.4)$$

$\overline{x}_{GK}$ is the calculated coordinate vector, A is the transformation matrix, x_{METRIC} and y_{METRIC} are the object coordinates in the image, α a is the rotation angle, P_{GK} is the centroid of the experimental plot in Gauss-Krueger system and n is the number of objects in the image. The rotation angle a is the azimuth between plot one and plot 54.

The objects were imported into ESRI (© ESRI, Redlands, California, USA) ArcGIS. Thirteen point shape file, according to the 13 recording dates, were directly created with the known objects Gauss-Krueger coordinates and the definition of the coordinate system. Along with the polygon shapes of the experimental plots an ArcGIS project was established. RUMOB distribution maps were created as points with varying diameter according to the actual object (leaf) area (Figure 5.1).

Based on the distribution maps RUMOB density maps were calculated, indicating the number of objects per square meter. Thereby, the GIS 'Kernel' density function was used to generate the density layers. Kernel density calculates the density of features in a search radius around those features. This function assigns greater importance to values near the kernel center and was implemented in ArcGIS Spatial Analyst. The radius for each density calculation was defined as one meter.

It became obvious, that most of the misclassifications were isolated small objects. However, RUMOB plants were exhibiting either large areas (due to overlapping leaves) or a number of small objects in higher densities (non-overlapping leaves of individual RUMOB plants). The combination of object area and density enabled a reduction of misclassification. This was accomplished by the condition, that either the object size increased 100 square centimeters or the density at this point increased beyond one object per square meter. The result is a binary raster with pixel values of one for pixels that fulfilled the conditions and zero for pixels that did not.

Finally, herbicide application maps were derived by labelling those plots to be sprayed that intersected objects fulfilling the above mentioned condition. By this means, we assumed that

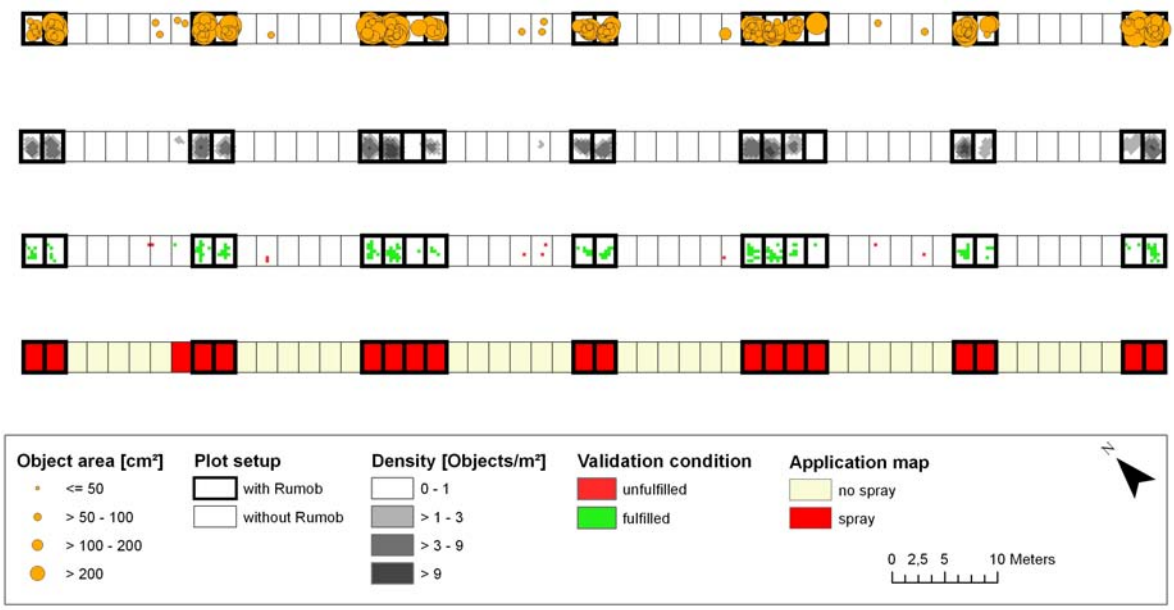

Figure 5.1.: *Derivation of herbicide application maps as demonstrated over 54 grass plots on the 12th of September in 2006. Size of objects classified as RUMOB in the images (the upper map) and object density (second from top) were combined for the reduction of misclassifications. The marked dots in the third map are identified misclassifications. Based on that, the herbicide application map (lower map) was calculated. Only those plots that intersected unmarked points are labelled to be sprayed. The plots with thick boundaries are those where RUMOB plants really appeared.*

each experimental plot is a partial area for site-specific treatment. Figure 5.1 illustrates the derivation of the herbicide application maps.

5.2.3. Quality assessment

With the classification results of all images, maps were calculated figuring the RUMOB distribution and the RUMOB application maps as time series. The quality of the classification was assessed. Therefore, plots which have been populated with RUMOB plants and were correctly assigned to be sprayed, were compared to those plots that have not been detected and those that were wrongly labelled to be sprayed. Rates of correctly detected RUMOB plots were achieved as well as the rates of misclassified non-RUMOB plots. Also, the apparent save of herbicide for each of the observation dates was calculated based on the herbicide maps.

5.3. Results

The image classification results for a plot with RUMOB plants are illustrated in Figure 5.3. Figures 5.4 and 5.5 show the distribution and application maps for 11 observation dates. Obviously the number of recognized RUMOB leaves decreased later during the first and second grassland growth, since the area of detected RUMOB objects increases and decreases during each of the two growths (Figures 5.2 and 5.3). In the first growing period, RUMOB objects (leaves) were correctly detected for the first three dates (May, 23rd - June 14th) only. The more vertical orientation of RUMOB leaves as compared to earlier growth stages and overlapping of leaves with grass blades disabled the detection of all leaves. There is a strong decrease in detected leave area from June 20th onwards (Figure 5.2), when overlapping with grasses begins. In the regrowths, the detection of plants was not possible before 15th of August (Figures 5.3 - 5.4), *i.e.* about five weeks after cut when the leaves exhibited a sufficient size for being detected by image segmentation. The area of detected RUMOB objects decreases with the last date, because more leaves became senescent.

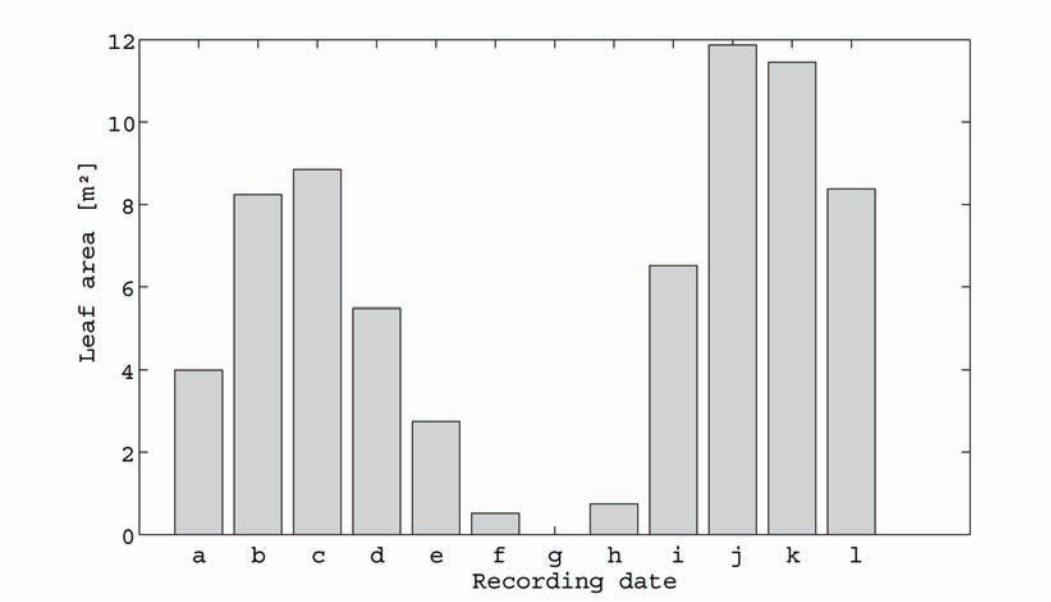

Figure 5.2.: *The change of object area for all RUMOB objects within the 18 RUMOB plots between on (a) May, 23. and (b) 29.05., (c) June 14., (d) 20., and (e) 26., July (f) 05., (g) 20., and (h) 31., August (i) 15. and (j) 29., September (k) 08., and (l) 12. in 2006.*

Table 5.1 shows the calculated classification accuracies, the error rates, and the theoretical save of herbicides. From May, 23rd until June, 26th and from August, 15th to September, 12th all 18 RUMOB plots have correctly been detected after mapping and post-processing, whereby the results for the 26th of June are irritating, because not all plants in the plots could successfully be segmented and thus could not be detected, because of the advanced plant growth with more vertical orientated leaves and overlapping. For this two time frames, the rate of wrongly classified plots (out of 36) varied from 19% - 58% after mapping and from 3% - 42% after post-processing, respectively. Given, that all experimental plots together would represent a paddock in a grassland farm in which RUMOB would have to be controlled, the maximum save of herbicide would have been 67%, equal to 18 experimental RUMOB plots out of 54. The GIS-based post-processing accounts for the biological proportions of typical RUMOB plant growing with more than one leaf per plant. The theoretical save of herbicides was 28% - 61% after mapping and 39% - 65% after post-processing.

High classification accuracies were achieved for most of the images taken over the two grassland growths. However, one has to take into account that the segmentation performance may and will decrease due to (i) overlapping of grasses with weed leaves and (ii) stronger image distortions with advanced plant growth. On the one hand, at the later growth stages some RUMOB plants thus could not be successfully detected. On the other hand, the earliest possible detection of RUMOB plants could be accomplished only when the leaves exhibited a size greater than 15 cm^2. The combination of object size (leaf area) and density (objects per square meter) further decreased misclassifications.

5.4. Discussion

Two time frames (May, 23rd until June, 20th and August, 15th to September, 12th) have been identified where image acquisition and classification provided reasonable results to identify RUMOB plants. However, the results varied strongly in both periods. For the first period higher misclassification (overestimation of RUMOB) could be observed within plot 1 to 18 (right to left in Figure 5.4). In these plots grass was sown in autumn 2005 while in the other it was sown one year before. All weeds however have been planted in spring 2005 in all of

Table 5.1.: *Classification results after image classification and GIS-based post processing. Number of detected RUMOB (R.o.) plots $n_{R.o.}$ (out of 18), the RUMOB plot detection rate $\%_{R.o.}$, number of plots misclassified as RUMOB n_{Error} (out of 36), the respective error rate $\%_{Error}$ and the theoretical reduction of herbicides $\%_{Save}$.*

DOY	After mapping					After post-processing				
	$n_{R.o.}$	$\%_{R.o.}$	n_{Error}	$\%_{Error}$	$\%_{Save}$	$n_{R.o.}$	$\%_{R.o.}$	n_{Error}	$\%_{Error}$	$\%_{Save}$
143	18	100	9	25	50	18	100	5	14	57
149	18	100	21	58	28	18	100	15	42	39
165	18	100	16	44	37	18	100	13	36	43
171	18	100	8	22	52	18	100	4	11	59
177	18	100	10	28	48	18	100	7	19	54
186	17	94	5	14	59	16	89	2	6	67
201	0	0	0	0	100	0	0	0	0	100
212	16	89	5	14	61	13	72	1	3	74
227	18	100	8	22	52	18	100	2	6	63
234	18	100	13	36	43	18	100	8	22	52
251	18	100	7	19	54	18	100	7	19	54
155	18	100	8	22	52	18	100	1	3	65

the 54 plots. In the 18 plots, the grasses were thus not as dense as in the other 36 and other herbs accompanied with RUMOB performed better growth and exhibited nontypical appearance, which resulted in higher confusion with RUMOB in the image classification. In the regrowth the grasses were well developed and classification mistakes were reduced. Same problems were faced with the last 8 plots were the grasses did not grow as proper as in the other plots, because of poor soil properties so that the weeds passed the grass sod more efficiently. Apart from that the errors are randomly distributed. The image classification procedure is a Maximum Likelihood Estimation, whereby for each image object the class is calculated to which it belongs most probably. Even if the probability of the right class is high, it might be possible that the belonging to another class is more probably. The image classification algorithm is not able to reduce the misclassification towards to zero. With the post-processing

however, some mistakes can be eliminated. Hence, for each of the investigated dates an increase of classification accuracy has been achieved with the GIS based post-classification applied.

Evaluating the 'time frames' from the plant phenological point of view it appeared that in both grassland growths best RUMOB detection was achieved from the 3-leaves stadium onwards. This is when the leaves were large enough to be separated from the background by the image segmentation. In contrast to the second grassland growth, in the first growths RUMOB plants were securely detected up to the 5 leaves stadium only. From then on, overlapping with other herbs reduced the detection accuracy. In the second growth the detection of RUMOB individuals performed well until the very last day of observation, where the plants had fully developed their rosette just before they start to flower. This developing stage of RUMOB would match with recommended application dates of selective herbicides when there is a maximum of herbicide absorption by the leaves (Kessler & Ammon, 1996; Zwerger & Ammon, 1999). Further, application of herbicides is recommended during under moderate temperatures up to 25°C which is case mostly during late summer.

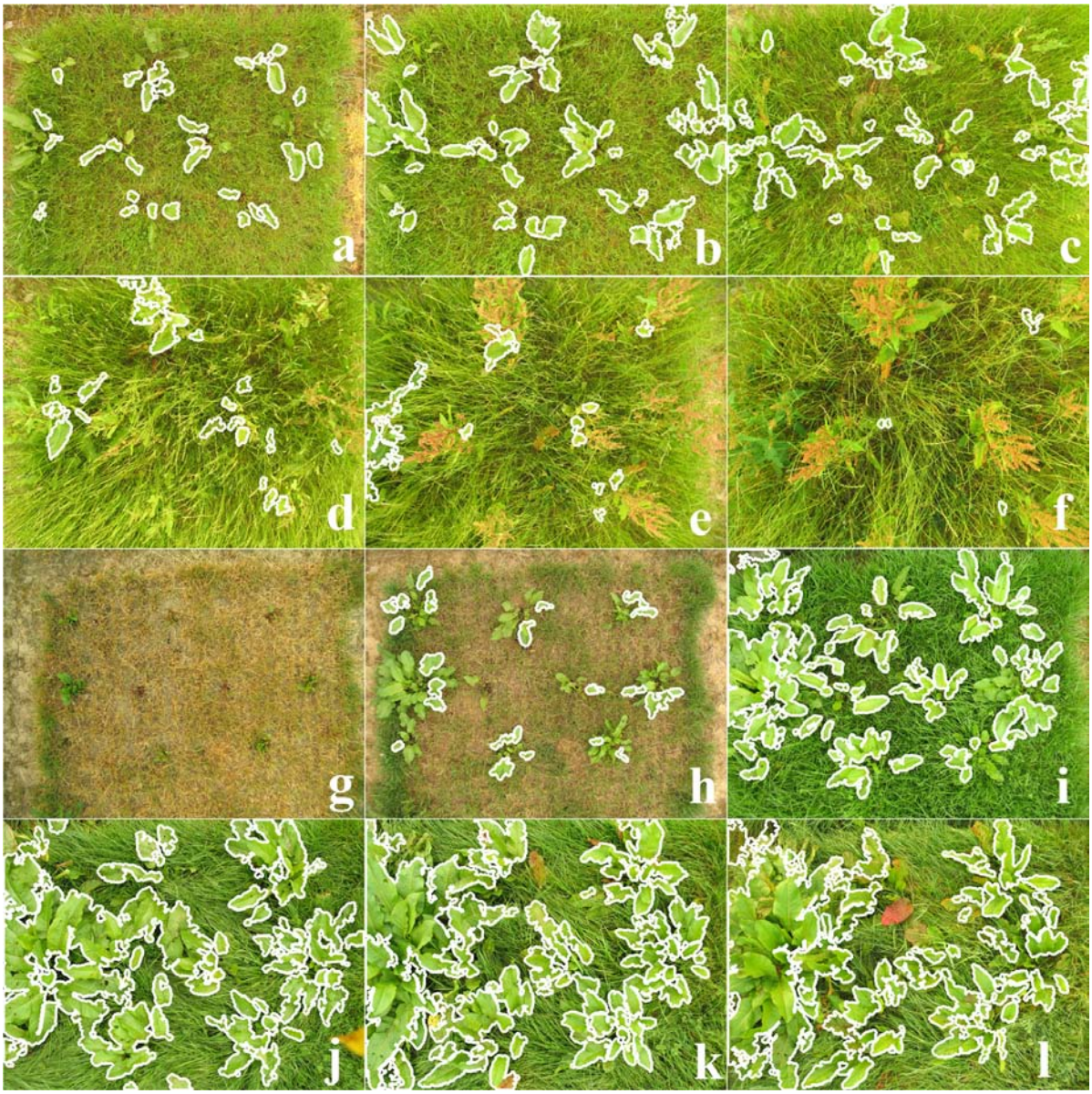

Figure 5.3.: *Example of one plot with results of automatic image classification for the images in the first growth: (a) May, 23. and (b) 29.05., (c) June 14., (d) 20., and (e) 26., July (f) 05.; and in the regrowth: (g) 20., and (h) 31., August (i) 15. and (j) 29., September (k) 08., and (l) 12. in 2006. Objects with thick white lines have been classified as RUMOB.*

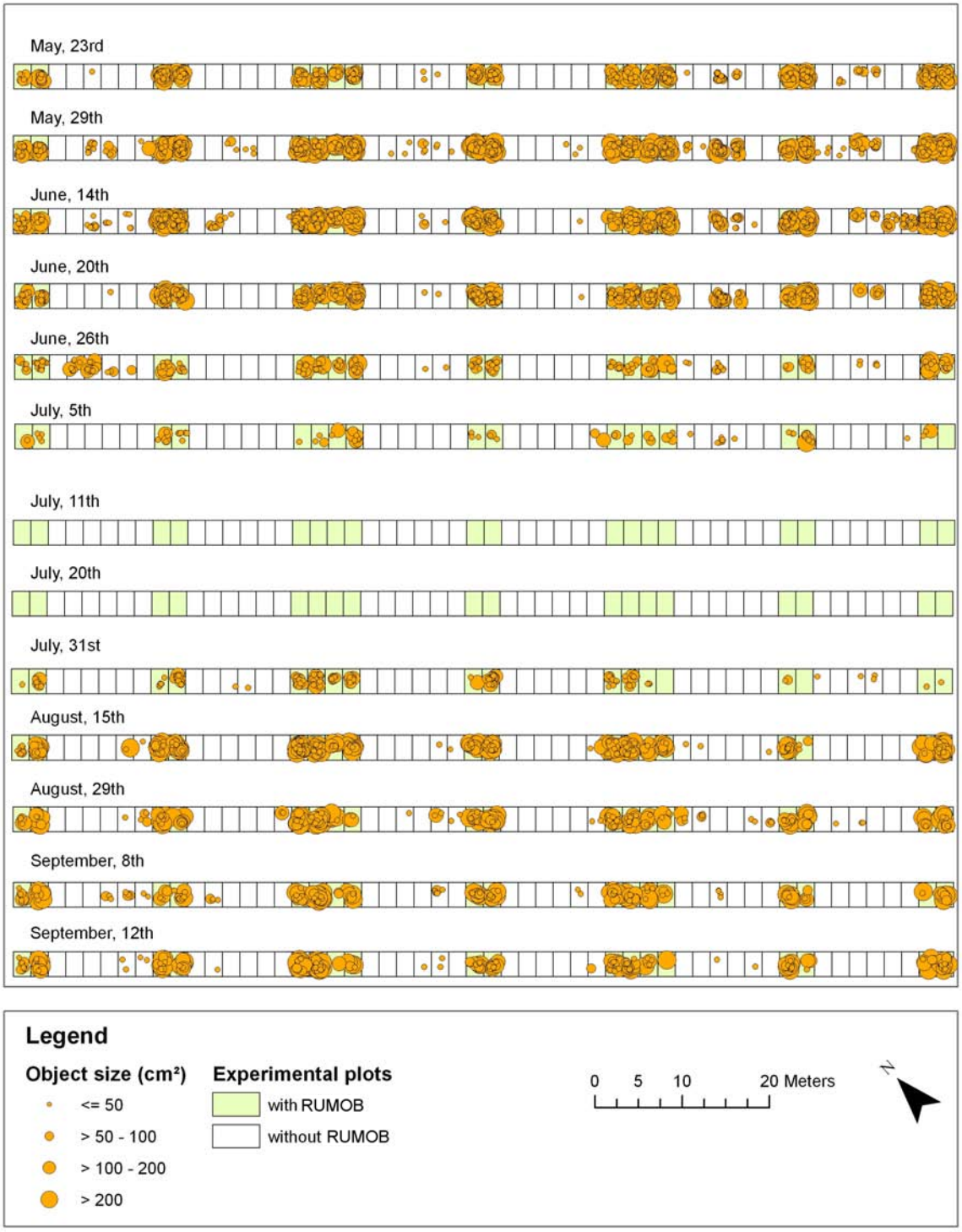

Figure 5.4.: *Distribution maps of image objects classified as RUMOB. Images have been acquired over two grassland growths in 2006*

Figure 5.5.: *The derived herbicide application maps against RUMOB as result of the combination of object area and density for each of the observed dates over both grassland growths in 2006*

6. Conclusions

Motivated by numerous investigations in arable crops, the aim of the doctoral study was to determine the possibilities and limitations of image analysis techniques for weed detection in grassland. The analysis was separated into different complementary experiments. The obtained results show high potential for the implementation of the system either in off-line or on-line systems for site-specific herbicide applications on grassland. In arable crops, the economic and environmental benefit through savings of herbicides by site-specific applications has already been demonstrated.

With the first experiment on this thesis, ground-based colour images were shown well suited for detecting grassland herbs. Previously, such systems were applied only to arable crops, where the studies concentrated on the discrimination between crop, weed and soil. Grassland is a much more complex background. Grass swards with mixtures of several herb species make the separation of weeds from the grass background more difficult. However, broad-leaved weeds are distinguishable from monocot grass by their larger homogeneous leaf surface. Where these leaves are not strongly overlapped the background grasses can be eliminated.

The developed image segmentation procedure in chapter 2 provided good segmentation of the weed leaves from the grassland background. Segmentation was done using a measure of homogeneity, the so called Local Homogeneity (Cheng & Sun, 2000), and morphological operations. Referring to publications on weed discrimination in arable crops (Lamb & Brown, 2001; Thorp & Tian, 2004), 5 geometrical, 3 colour, and 1 texture feature(s) were calculated for the remaining image objects. A Maximum Likelihood classificator for discriminating the weed species *Rumex obtusifolius* L., *Taraxacum officinale* Web., and *Plantago major* L. and a soil- and residue class was established. All images taken under constant geometric and illumination conditions at three dates in July 2005 were classified. Total classification accuracy ranged

from 65% to 81%. The rate of correctly detected RUMOB objects was between 71% and 87%. Detection appeared to be decreasing with time, indicating a change in phenology and morphology creating a change in geometric features.

In this investigation one source of error was high confusion of PLAMA objects with RUMOB. Also the negative effect of image distortions in the segmentation and with that wrongly segmented objects increased the error. The classification result was further determined by different feature combinations. Although object geometry did not contribute strongly to the classification accuracy, its integration into the classification procedure gave the best classification results. Combining the texture with the colour features gave classification accuracies close to those with all features.

Based on the results and conclusions of chapter 2 more colour and texture features were calculated. The modified image classification procedure described in 3 increased the accuracy of *Rumex obtusifolius* L. detection and minimized the misclassification. Using stepwise discriminant analysis, colour and texture were the two features identified as key contributors to classification, whereas geometric features appeared irrelevant for the classification. Geometry is widely used in arable crops to identify weed species as young seedlings, and such systems fail when plants overlap at the later stages of growth. In grassland, overlapping of plants is the norm. Consequently, one can expect shape properties to play a minor role in grassland plant identification. In general, the rates of detection obtained for RUMOB were large (up to 95%) with few objects from other classes misclassified as RUMOB. It is worth noting that an individual RUMOB plant comprises more than one object in the images; its leaves are the objects that are segmented (provided that they do not overlap) and so the rate of correctly detected *Rumex* plants can be assumed to be significantly higher than the object detection rates.

The image analysis was quite slow. Images were processed offline because the processing speed is too slow for on-line techniques in precision agriculture. Digital images require considerable computer memory. In this study, most time elapsed in the conversion of RAW to TIFF images and in image segmentation, especially when calculating the local homogeneity image. With reduced image resolution the time of processing must decrease.

The experiment described in chapter 4 was conducted to analyse the impact of reduced im-

age resolutions on the classification results. At the same time, the negative effect of distortions in the segmentation procedure was eliminated by defining a confidence circle around the image centre. Only those objects falling into this confidence area were considered for classification. The segmentation algorithm was applied successfully to different image resolutions. The number of segmented RUMOB objects was approximately the same at all resolutions. Although the number of wrongly segmented objects increased at the lower resolutions, this did not affect the classification results adversely. For all image resolutions, large RUMOB detection rates were achieved. The lowest classification accuracies were for images with resolutions of 1024 $\times$ 1280 pixels and 768 $\times$ 1024 pixels, although they were still high. Surprisingly, classification of the images with the lowest resolution were ranked third when comparing all results using the classification quality index. For the lowest image resolution the time required for image segmentation, feature extraction and classification was less than 3 seconds. For full resolution images more than 45 seconds was required.

The last experiment (chapter 5) was conducted on data obtained continuously over two grassland growths in 2006. All captured images were rescaled to 480 $\times$ 640 pixels according to the results from chapter 4. Image classification was performed automatically using the developed '*Rumex* detection toolbox'. The coordinates of the image objects classified as RUMOB were transformed to Gauss-Krueger coordinate system and imported into GIS software. With that, distribution maps of every observation date were created. Those were compared to the reality measured in the field experiment. It became obvious that most misclassification was due to isolated small objects. The combination of object area and density allowed for a minimization of those errors. With that post-processing technique the quality of the RUMOB maps were increased in terms of correctness. As result of this experiment, all plots with *Rumex obtusifolius* L. have been detected within specific time frames (May, 23rd until June, 20th and from August, 15th to September, 12th) during the growing season 2006. The error rate of plots without RUMOB but classified as RUMOB in these two time frames (containing 8 data sets in total) was between 3% and 42% resulting in theoretical herbicide saves of 39% - 65% as compared to conventional application of the whole field. The best results with lowest misclassification were achieved on September 12th, when most selective herbicides against *Rumex obtusifolius* L. are beeing recommended for application for instance during late summer where the leaf rosette is

fully established and the plants start to flower, as it was the case on the 12th of September.

The classification procedure was implemented in a software called '*Rumex* detection toolbox (RDT)', a MATLAB (© The Mathworks, Inc.) based graphical user interface for batch processing of image data sets. The results can be exported as tables. Also the software allows for an export of RUMOB object coordinates which can be further used in GIS software for mapping the distribution of RUMOB individuals and to further minimize the misclassification as presented in the last experiment. Within GIS herbicide application maps can simply be derived.

Even though the classification results are very much satisfying, one has to take into consideration that the images used for algorithm development and testing have been captured under constant light conditions. Image recording was dome during cloudy conditions and were not disturbed by direct sunlight, which will in fact always be a problem due to shadows or strong reflections of the vegetation. To overcome these problems, the execution of image collection can take place under cloudy conditions or even in night. The image acquisition unit equipped with artificial light sources then may ensure a constant illumination during image recording.

Future studies will develop the application technology. An image acquisition unit mounted on a tractor for weed detection in real field conditions has already been started. This new unit consists of two high speed industrial colour cameras mounted in front of a driving tractor. Images are Global Positioning System (GPS) referenced and will completely cover the investigated field. With a short time delay, a spray application can follow behind the tractor, equipped with a spraying device allowing for a high spatial resolution herbicide application.

References

Aitkenhead, M. J., Dalgetty, I. A., Mullins, C. E., McDonald, A. J. S., & Strachan, N. J. C. 2003. Weed and crop discrimination using image analysis and artificial intelligence methods. *Computers and Electronics in Agriculture*, **39**(3), 157–171.

Bonesmo, H., Kaspersen, K., & Bakken, A. K. 2004. Evaluating an image analysis system for mapping white clover pastures. *Acta Agriculturae Scandinavica, Section B - Soil and Plant Science*, **54**(2), 76–82.

Brivot, R., & Marchant, J. A. 1996. Segmentation of plants and weeds for a precision crop protection robot using infrared images. *Iee Proceedings-Vision Image and Signal Processing*, **143**(2), 118–124.

Burks, T. F., Shearer, S. A., & Payne, F. A. 2000. Classification of weed species using color texture features and discriminant analysis. *Transactions of the Asae*, **43**(2), 441–448.

Burks, T. F., Shearer, S. A., Heath, J. R., & Donohue, K. D. 2005. Evaluation of neural-network classifiers for weed species discrimination. *Biosystems Engineering*, **91**(3), 293–304.

Cavers, P. B., & Harper, J. L. 1964. Rumex-Obtusifolius L and R-Crispus L. *Journal of Ecology*, **52**(3), 737–766.

Cheng, H. D., & Sun, Y. 2000. A hierarchical approach to color image segmentation using homogeneity. *Ieee Transactions on Image Processing*, **9**(12), 2071–2082.

Dicke, D., Fries, A., & Gerhards, R. 2004. Determination of weed thresholds for site-specific weed control in malting barley. *Zeitschrift für Pflanzenkrankheiten und Pflanzenschutz - Journal of Plant Diseases and Protection*, **Special Issue XIX**, 413–421.

Dicke, D., Gerhards, R., Buchse, A., & Hurle, K. 2007. Modeling spatial and temporal dynamics of Chenopodium album L. under the influence of site-specific weed control. *Crop Protection*, **26**(3), 206–211.

Du, C. J., & Sun, D. W. 2004. Recent developments in the applications of image processing techniques for food quality evaluation. *Trends in Food Science and Technology*, **15**(5), 230–249.

Duda, Richard O., Hart, Peter Elliot, & Stork, David G. 2001. *Pattern classification.* 2. ed edn. New York, USA: Wiley.

Elsässer, Martin. 2004. Das Übel an der Wurzel packen. *DLZ Sonderheft, Grünlandpraxis für Profis*, 38–42.

Everitt, J. H., Ingle, S. J., Gausman, H. W., & Mayeux, H. S. 1984. Detection of False Broomweed (Ericameria-Austrotexana) by Aerial-Photography. *Weed Science*, **32**(5), 621–624.

Everitt, J. H., Pettit, R. D., & Alaniz, M. A. 1987. Remote-Sensing of Broom Snakeweed (Gutierrezia-Sarothrae) and Spiny Aster (Aster-Spinosus). *Weed Science*, **35**(2), 295–302.

Everitt, J. H., Alaniz, M. A., Escobar, D. E., & Davis, M. R. 1992. Using Remote-Sensing to Distinguish Common (Isocoma-Coronopifolia) and Drummond Goldenweed (Isocoma-Drummondii). *Weed Science*, **40**(4), 621–628.

Everitt, J. H., Escobar, D. E., Villarreal, R., Alaniz, M. A., & Davis, M. R. 1993. Canopy Light Reflectance and Remote-Sensing of Shin Oak (Quercus-Havardii) and Associated Vegetation. *Weed Science*, **41**(2), 291–297.

Everitt, J. H., Anderson, G. L., Escobar, D. E., Davis, M. R., Spencer, N. R., & Andrascik, R. J. 1995. Use of Remote-Sensing for Detecting and Mapping Leafy Spurge (Euphorbia-Esula). *Weed Technology*, **9**(3), 599–609.

Franz, E., Gebhardt, M. R., & Unklesbay, K. B. 1991a. Shape-Description of Completely Visible and Partially Occluded Leaves for Identifying Plants in Digital Images. *Transactions of the Asae*, **34**(2), 673–681.

Franz, E., Gebhardt, M. R., & Unklesbay, K. B. 1991b. The Use of Local Spectral Properties of Leaves as an Aid for Identifying Weed Seedlings in Digital Images. *Transactions of the Asae*, **34**(2), 682–687.

Galler, Josef. 1989. *Grünlandverunkrautung : Ursachen, Vorbeugung, Bekämpfung*. Praxisbuch Pflanzenbau. Graz, Austria: Leopold Stocker Verlag.

Gerhards, R., & Oebel, H. 2006. Practical experiences with a system for site-specific weed control in arable crops using real-time image analysis and GPS-controlled patch spraying. *Weed Research*, **46**(3), 185–193.

Gerhards, R., Sökefeld, M., Schulze Lohne, K., Mortensen, D. A., & Kühbauch, W. 1997. Site specific weed control in winter wheat. *Journal of Agronomy and Crop Science*, **178**(4), 219–225.

Gerhards, R., Sökefeld, M., Timmermann, C., Krohmann, P., & Kühbauch, W. 2000. Precision Weed Control - more than just saving herbicides. *Journal of Plant Diseases and Protection*, **Special Issue XVII**, 179–186.

Gerhards, R., Sökefeld, M., Nabout, A., Therburg, R.-D., Krohmann, P., Timmermann, C., & Kühbauch, W. 2002. Online weed control using digital image analysis. *Journal of Plant Diseases and Protection*, **Special Issue XVIII**, 421–427.

Glenn, Nancy F., Mundt, Jacob T., Weber, Keith T., Prather, Timothy S., Lass, Lawrence W., & Pettingill, Jeffrey. 2005. Hyperspectral data processing for repeat detection of small infestations of leafy spurge. *Remote Sensing of Environment*, **95**(3), 399–412.

Gonzales, Rafael C., & Woods, Richard E. 1992. *Digital image processing*. 3. edn. Reading, Massachusetts, USA: Addison-Wesley.

Hemming, J., & Rath, T. 2001. Computer-vision-based weed identification under field conditions using controlled lighting. *Journal of Agricultural and Engineering Research*, **78**(3), 233–243.

Hoppe, J. H. 2007. *Unkrautbekämpfung im Dauergrünland.* http://www.lwk-niedersachsen.de/download.cfm/file/507,pflanzenschutz_gruenland˜pdf.html. *(Last checked on 02-May-2007).*

Jia, J., & Krutz, G. W. 1992. Location of the Maize Plant with Machine Vision. *Journal of Agricultural Engineering Research*, **52**(3), 169–181.

Kavdir, I. 2004. Discrimination of sunflower, weed and soil by artificial neural networks. *Computers and Electronics in Agriculture*, **44**(2), 153–160.

Kessler, & Ammon. 1996. Wiesenblacke und Alpenblacke. Eigenschaften, Hauptursache, Bekämpfung. *Merkblatt Nr. 7 der Arbeitsgemeinschaft zur Förderung des Futterbaus (AGGF).*

Lamb, Weedon, & Rew. 1999. Evaluating the accuracy of mapping weeds in seedling crops using airborne digital imaging: Avena spp. in seedling triticale. *Weed Research*, **39**.

Lamb, D. W., & Brown, R. B. 2001. Remote-sensing and mapping of weeds in crops. *Journal of Agricultural Engineering Research*, **78**(2), 117–125.

Lopez-Granados, F., Jurado-Exposito, M., Pena-Barragan, J. M., & Garcia-Torres, L. 2006. Using remote sensing for identification of late-season grass weed patches in wheat. *Weed Science*, **54**(2), 346–353.

Marchant, J. A., & Onyango, C. M. 2003. Comparison of a Bayesian classifier with a multilayer feed-forward neural network using the example of plant/weed/soil discrimination. *Computers and Electronics in Agriculture*, **39**(1), 3–22.

Marchant, J. A., Tillett, R. D., & Brivot, R. 1998. Real-time segmentation of plants and weeds. *Real-Time Imaging*, **4**(4), 243–253.

Menges, R. M., Nixon, P. R., & Richardson, A. J. 1985. Light Reflectance and Remote-Sensing of Weeds in Agronomic and Horticultural Crops. *Weed Science*, **33**(4), 569–581.

Meyer, G. E., Mehta, T., Kocher, M., Mortensen, D. A., & Samal, A. 1998. Textural imaging

and discriminant analysis for distinguishing weeds for spot spraying. *Transactions of the Asae*, **41**(4), 1189–1197.

Neto, J. C., Meyer, G. E., Jones, D. D., & Samal, A. K. 2006. Plant species identification using Elliptic Fourier leaf shape analysis. *Computers and Electronics in Agriculture*, **50**(2), 121–134.

Niggli, Urs. 1985. *Bekämpfung von Rumex obtusifolius L. und Bestandeslenkung in intensiv bewirtschafteten Naturwiesen.* Dissertation, ETH Zürich, 7757.

Onyango, C., Marchant, J., Grundy, A., Phelps, K., & Reader, R. 2005. Image processing performance assessment using crop weed competition models. *Precision Agriculture*, **6**(2), 183–192.

Perez, A. J., Lopez, F., Benlloch, J. V., & Christensen, S. 2000. Colour and shape analysis techniques for weed detection in cereal fields. *Computers and Electronics in Agriculture*, **25**(3), 197–212.

Petry, W., & Kühbauch, W. 1989. Automatic distinction of weed species using form parameters by means of digital image processing. *Journal of Agronomy and Crop Science*, **163**(5), 345–351.

Pötsch, E.M. 2001. Wissenswertes zur mechanischen und chemischen Ampferbekämpfung. *Pages 75–81 of: Bericht über das 7. Alpenländische Expertenforum zum Thema "Bestandesführung und Unkrautregulierung im Grünland - Schwerpunkt Ampfer".* Irdning: Bundesanstalt für alpenländische Landwirtschaft Gumpenstein.

Richardson, A. J., Menges, R. M., & Nixon, P. R. 1985. Distinguishing Weed from Crop Plants Using Video Remote-Sensing. *Photogrammetric Engineering and Remote Sensing*, **51**(11), 1785–1790.

Shearer, S. A., & Holmes, R. G. 1990. Plant-Identification Using Color Cooccurrence Matrices. *Transactions of the Asae*, **33**(6), 2037–2044.

Soille, P. 2000. Morphological image analysis applied to crop field mapping. *Image and Vision Computing*, **18**(13), 1025–1032.

Stafford, J. V., & Miller, P. C. H. 1993. Spatially selective application of herbicide to cereal crops. *Computers and Electronics in Agriculture*, **9**(3), 217–229.

Stafford, J. V., Le Bars, J. M., & Ambler, B. 1996. A hand-held data logger with integral GPS for producing weed maps by field walking. *Computers and Electronics in Agriculture*, **14**(2-3), 235–247.

Stork, David G., Yom-Tov, Elad, & Duda, Richard O. 2004. *Computer manual in MATLAB to accompany Pattern Classification*. 2nd edn. Hoboken, USA: Wiley-Interscience.

Tamura, H., Atoda, O., & Sakai, K. 2000. Texture analysis method to distinguish clover stocks from grass thicket. *Pages 309–314 of: Proceedings of the 4th Asia-Pacific Conference on Control and Measurement.*

Thorp, K. R., & Tian, L. F. 2004. A review on remote sensing of weeds in agriculture. *Precision Agriculture*, **5**(5), 477–508.

Tian, L. F., & Slaughter, D. C. 1998. Environmentally adaptive segmentation algorithm for outdoor image segmentation. *Computers and Electronics in Agriculture*, **21**(3), 153–168.

Tillett, Nick D., Hague, T., & Miles, S. J. 2001. A field assessment of a potential method for weed and crop mapping on the basis of crop planting geometry. *Computers and Electronics in Agriculture*, **32**(3), 229–246.

Woebbecke, D. M., Meyer, G. E., Vonbargen, K., & Mortensen, D. A. 1995a. Color Indexes for Weed Identification under Various Soil, Residue, and Lighting Conditions. *Transactions of the Asae*, **38**(1), 259–269.

Woebbecke, D. M., Meyer, G. E., Vonbargen, K., & Mortensen, D. A. 1995b. Shape-Features for Identifying Young Weeds Using Image-Analysis. *Transactions of the Asae*, **38**(1), 271–281.

Zaller, J. G. 2004. Ecology and non-chemical control of Rumex crispus and R. obtusifolius (Polygonaceae): a review. *Weed Research*, **44**(6), 414–432.

Zhang, N., & Chaisattapagon, C. 1995. Effective Criteria for Weed Identification in Wheat Fields Using Machine Vision. *Transactions of the Asae*, **38**(3), 965–974.

Zwerger, Peter, & Ammon, Hans-Ulrich. 1999. *Unkraut - Ökologie und Bekämpfung.* Verlag Eugen Ulmer.

List of Figures

List of Tables

List of Acronyms

CCD Charge-Coupled Device

CCM Colour Co-occurrence Method

DOY Day Of Year

GIS Geographic Information System

GPS Global Positioning System

GUI Graphical User Interface

JPEG Joint Photographic Experts Group

MANOVA Multivariate ANalysis Of VAriance

MLE Maximum Likelihood Estimation

NTSC National Television System Committee

PLAMA *Plantago major* L.

RDT *Rumex* Detection Toolbox

RUMOB *Rumex obtusifolius* L.

SE Structure Element

SPSS Statistical Product and Service Solutions

TAROF *Taraxacum officinale* Web.

TIFF Tagged Image File Format

A. List of Publications

Peer-reviewed journals

Gebhardt, S., Schellberg, J., Lock, R. and Kühbauch, W., 2006. Identification of broad-leaved dock (*Rumex obtusifolius* L.) on grassland by means of digital image processing. Precision Agriculture, 7(3): 165-178.

Gebhardt, S. and Kühbauch, W., 2007. A new algorithm for automatic *Rumex obtusifolius* detection in digital images using colour and texture features and the influence of image resolution. Precision Agriculture, 8(1-2): 1-13.

Conference proceedings

Gebhardt, S. and Kühbauch, W., 2005. Untersuchungen zur Unkrauterkennung im Grünland mittels digitaler Bildverarbeitung. In: B. Herold (Editor), 11. Workshop Computer-Bildanalyse in der Landwirtschaft. Bornimer Agrartechnische Berichte, Potsdam-Bornim, Germany, pp. 124-130.

Gebhardt, S. and Kühbauch, W., 2005. Chancen der Ampfererkennung mittels digitaler Bildverarbeitung, 49. Jahrestagung der Arbeitsgemeinschaft Grünland und Futterbau (AGGF). Tagungsband, Bad-Elster, Germany, pp. 69-72.

Gebhardt, S. and Kühbauch, W., 2006. Image analysis for automatic classification of *Rumex obtusifolius* in mixed grassland swards. Journal of Plant Diseases and Protection, Special Issue XX: 189-195.

Gebhardt, S. and Kühbauch, W., 2006. Automatic detection of *Rumex obtusifolius* by digital imaging. In: J. Lloveras *et al.* (Editors), 21st General Meeting of the European Grassland Federation. Grassland Science in Europe: Sustainable Grassland Productivity. Organizing Committee of the 21st General Meeting of the European Grassland Federation, Badajoz, Spain, pp. 574-576.

Gebhardt, S. and Kühbauch, W., 2006. Ein bildanalytischer Ansatz zur Ampferdetektion. In: B. Herold (Editor), 12. Workshop Computer-Bildanalyse in der Landwirtschaft. Bornimer Agrartechnische Berichte, Bonn, Germany, pp. 7-15.

Gebhardt, S. and Kühbauch, W., 2006. Image classification approach for automatic identification of grassland weeds. In: W. Gao and S.L. Ustin (Editors), Remote Sensing and Modeling of Ecosystems for Sustainability III. SPIE, San Diego, CA, USA, pp. 629806-8.

Gebhardt, S. and Kühbauch, W., 2006. Automatische Detektion und Kartierung von Stumpfblättrigem Ampfer (*Rumex obtusifolius* L.) mit digitaler Kameratechnik und Bildkonversion., 50. Jahrestagung der Arbeitsgemeinschaft Grünland und Futterbau (AGGF). Schriftenreihe der Bayerischen Landesanstalt für Landwirtschaft. LfL, Straubing, Germany, pp. 34-37.

Gebhardt, S. and Kühbauch, W., 2007. Continous mapping of *Rumex obtusifolius* during different growing periods based on automatic image classification and GIS-based post-processing. In: J. Stafford (Editor), Precision Agriculture '07, Proceedings on the 6th European Conference on Precision Agriculture, Skiathos, Greece, pp. 499-506.

B. *Rumex* detection toolbox (RDT)

The *Rumex* Detection Toolbox (RDT) (Figure B.1) is a MATLAB (© The Mathworks, Inc.) based Graphical User Interface (GUI) especially designed for the batch processing of images used in this thesis. In general the RDTs processing design is following a four-steps approach which are: (1) selection of images to be classified; (2) training the classifier; (3) classification of images; and (4) export of classification results.

When starting RDT a start frame shows up (Figure B.1). The only button enable to be pressed is the *'Select images'* button. Clicking the button opens the image file dialogue (Figure B.2). A filter enables the selection of the Joint Photographic Experts Group (JPEG) (*.jpg, *.jpeg) format and TIFF (*.tif;*.tiff). There is no limitation in the number of images that can be selected.

With the finishing of the image file selection the RDT enables the *'Train classifier'* button. Starting from the root directory of the RDT the user has the possibility to choose between a variety of training data sets within the 'training' folder (Figure B.3). With the current version training data sets are available for the three common image resolutions: (1) 2448 × 3264; (2) 1200 × 1600; and (3) 480 × 640, available through the respective subdirectories. All training data sets are Matlab files (*.mat). Within these files two variables are stored which are *'patterns'* and *'targets'*. *patterns* is a 12 by n matrix with the 12 colour and texture features for n objects. *targets* is a vector with the respective class membership for each of the n objects. Within each subdirectory 6 training data sets are available. Three of them define classifiers for the 5 classes RUMOB, PLAMA, TAROF, SOIL, and RESIDUE. The remaining three files define classifications into the 4 classes RUMOB, PLAMA, TAROF/RESIDUE, and SOIL. The three training data sets within each of these subgroups origin from different recording dates in July 2005. The date is coded in the file name as 'day after cut'. With the training data set

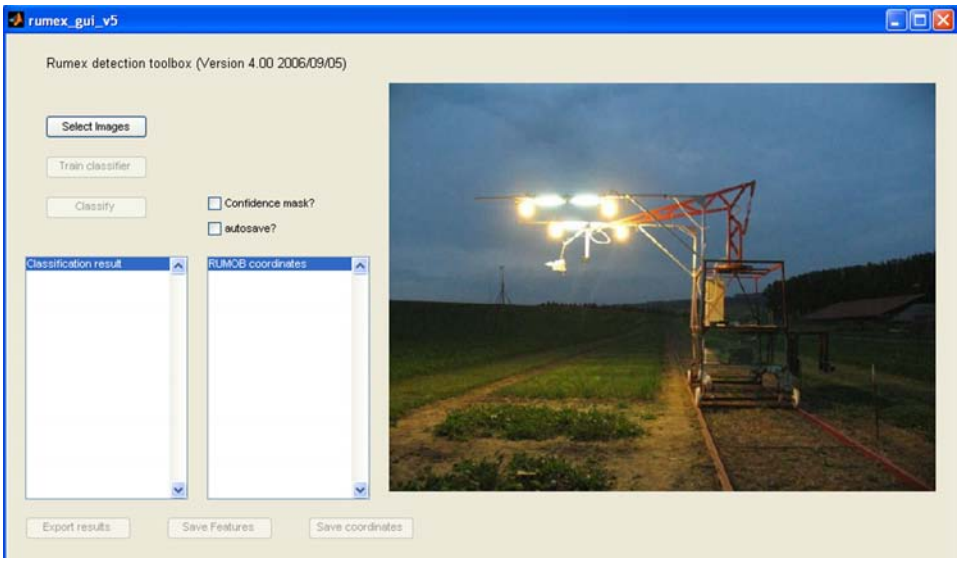

Figure B.1.: *The RDT start screen.*

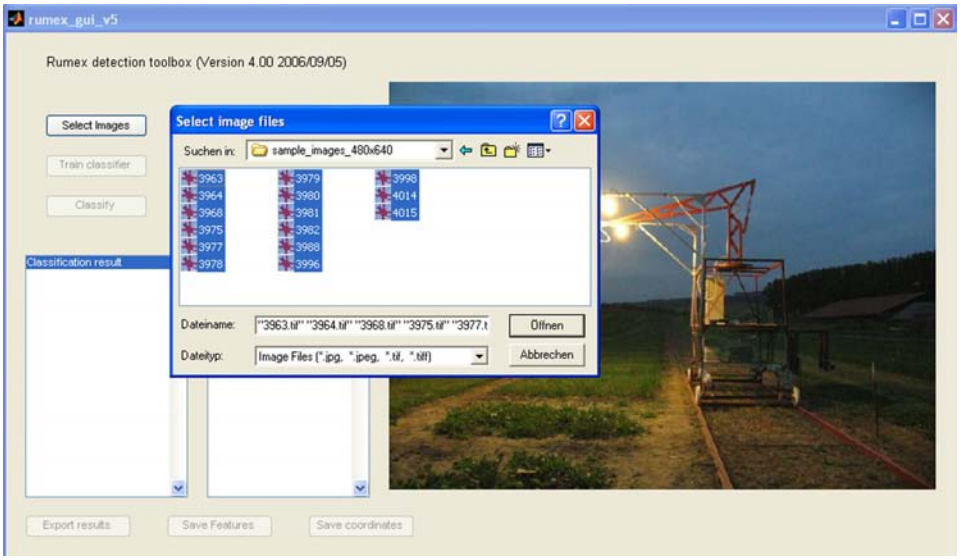

Figure B.2.: *RDT Image file selection dialogue*

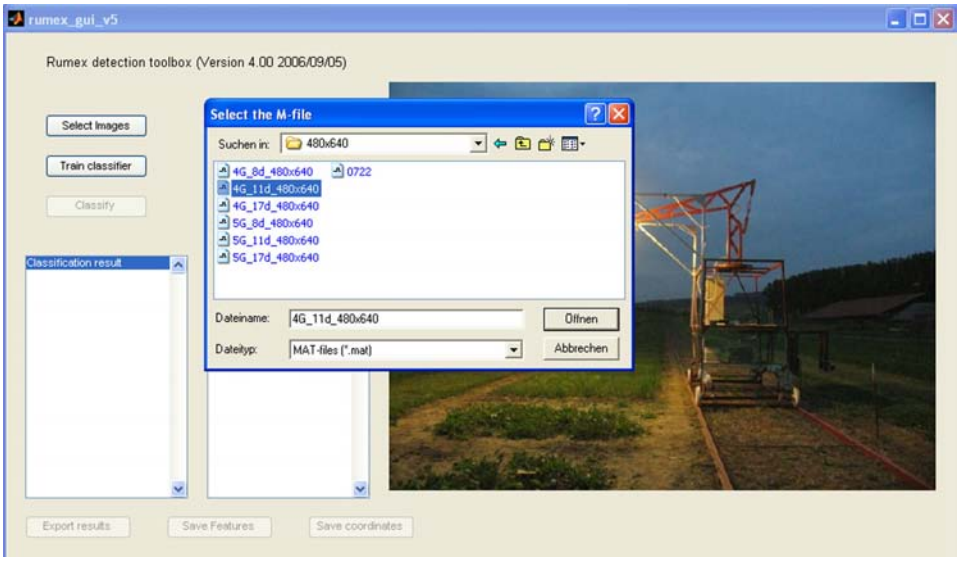

Figure B.3.: *RDT training data set selection dialogue*

'4G_8d_480x640.mat' for example, an training data set for a classification into 4 groups (4G), derived 8 days after cut (8d) for an image resolution of 480 × 640 pixels is available. The suggested training data set for all classifications is the one derived 11 days after cut, which is the July 22nd data set, which has most frequently been used in this thesis.

After training the classifier the image classification can be performed. Before doing so, the user should select whether he wants the confidence mask to be applied (see Chapter 4) and whether he wants the annotated classified images to be automatically stored on the computer. Both options can be enabled using the respective checkboxes in the RDT GUI.

With the activating of the *'Classify'* button the user has to define the output directory of the annotated images (Figure B.4). The processing of the images is then started. The information which image is currently processed is written to the GUI. After an image is processed it is visualised in the GUI along with the annotated classification results, where red contours show those image objects classified as RUMOB (Figure B.5). Also, the confidence mask is drawn in white, independent from whether is was chosen by the user or not. The number of objects found in the image is shown in the left table of the GUI. The results for each image are written to a new row. Each row consists of the number of objects found for each of the four or five classes. The right table comprises the image coordinates for each individual RUMOB object

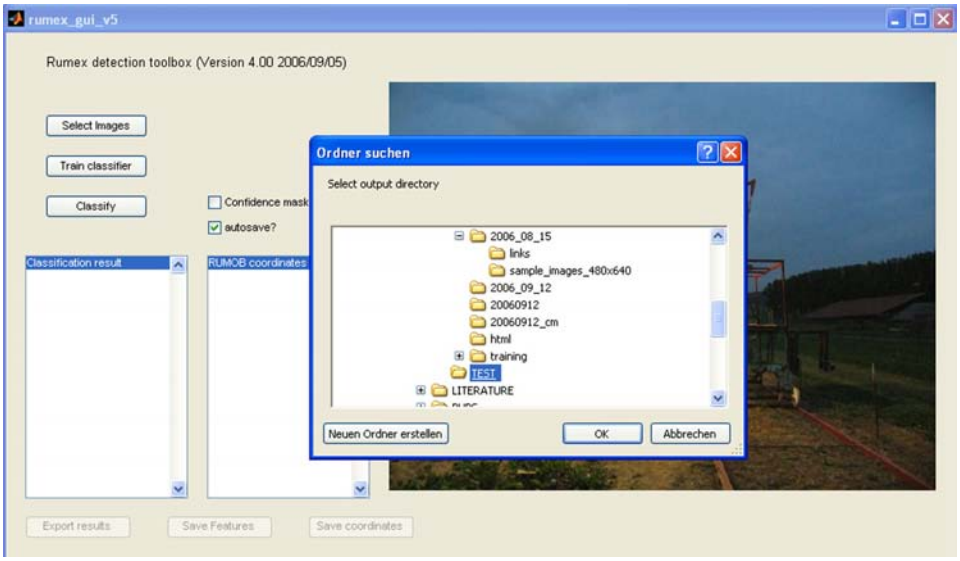

Figure B.4.: *RDT autosave folder selection dialogue*

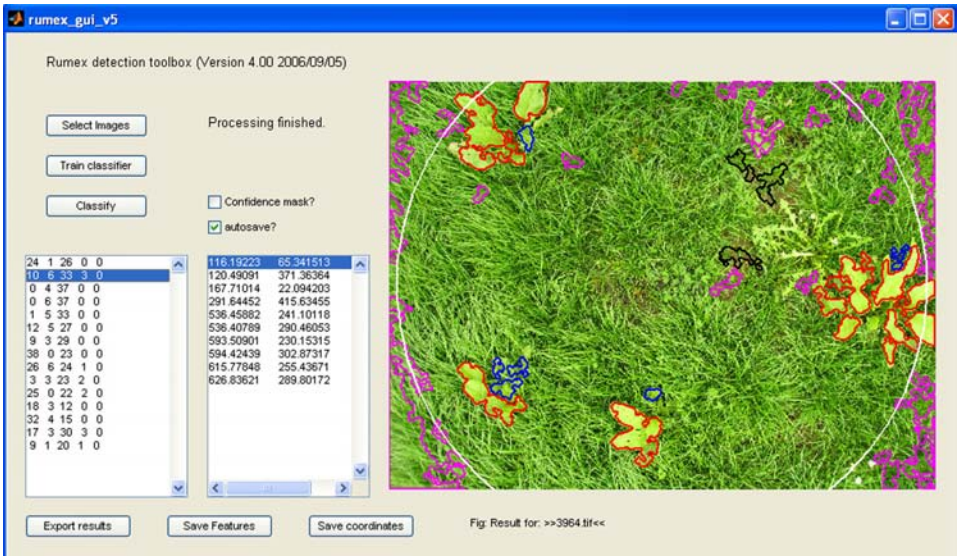

Figure B.5.: *Annotated images showing result of classification*

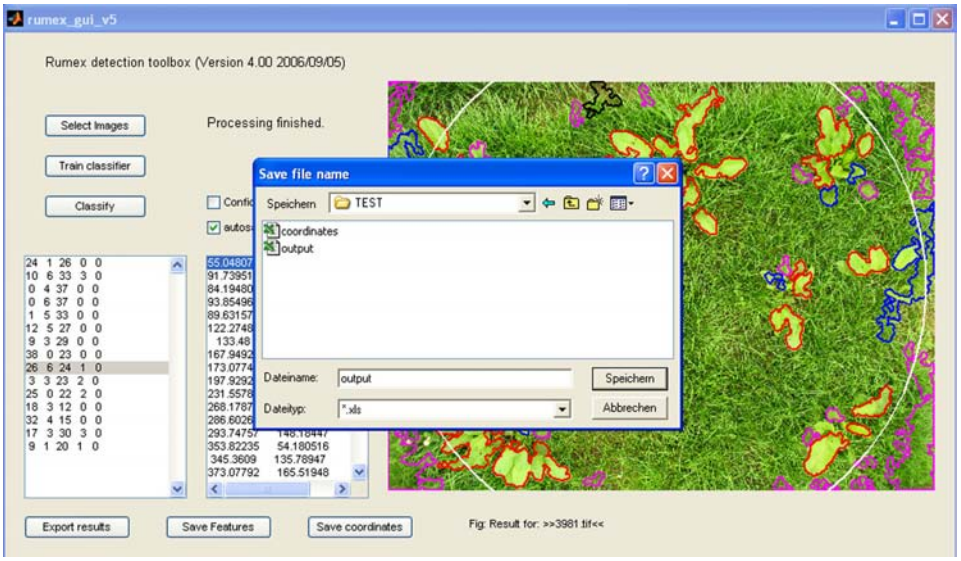

Figure B.6.: *RDT export results dialogue*

in the current image along with its size. After the processing of all images has been completed the classification results for each information can be accessed by clicking on the respective row in the left table.

There are three export modules available with the RDT. First, the results shown in the left table can be exported to an Microsoft (© Microsoft, Inc.) Excel data sheet (Figures B.6 and B.7) using the *'Export results'* button. In the same way, the coordinates of all RUMOB objects can be exported to an Excel data sheet by clicking the *'Save coordinates'* button. In addition to the image coordinates the calculated metric coordinates (in mm) and the area (in mm^2) are stored. With the image id results can be related to the corresponding input image. Alternatively all results can be stored to a Matlab file using the *'Save features'* button. With that, all results are available within Matlab, which are all object features *(featlist)*, coordinates *(RCOORD)*, boundary coordinates *(boundlist)*, areas *(arealist)* and calculated class memberships *(classlist)*. The *RCOORD* variable is also input for the subsequent mapping of RUMOB objects.

	A	B	C	D	E	F
1	Filename	N_RUMOB	N_TAROF/Res.	N_PLAMA	N_SOIL	N_RESID
2	3963.tif	24	1	26	0	0
3	3964.tif	10	6	33	3	0
4	3968.tif	0	4	37	0	0
5	3975.tif	0	6	37	0	0
6	3977.tif	1	5	33	0	0
7	3978.tif	12	5	27	0	0
8	3979.tif	9	3	29	0	0
9	3980.tif	38	0	23	0	0
10	3981.tif	26	6	24	1	0
11	3982.tif	3	3	23	2	0
12	3988.tif	25	0	22	2	0
13	3996.tif	18	3	12	0	0
14	3998.tif	32	4	15	0	0
15	4014.tif	17	3	30	3	0
16	4015.tif	9	1	20	1	0
17	3999.tif	36	1	16	0	0
18	4000.tif	0	6	10	0	0
19	4001.tif	0	2	11	0	0
20	4002.tif	0	0	14	0	0
21	4003.tif	0	2	13	0	0
22	4004.tif	0	2	11	0	0
23	4005.tif	0	0	12	1	0
24	4006.tif	19	0	4	0	0
25	4007.tif	22	0	6	0	0

Figure B.7.: *Exported table showing results of classified images*

C. RDT Matlab source codes

rumex_gui_v5.m

```
function varargout = rumex_gui_v5(varargin)
% RUMEX_GUI_V5 M-file for rumex_gui_v5.fig

% Begin initialization code - DO NOT EDIT
gui_Singleton = 1;
gui_State = struct('gui_Name',       mfilename, ...
                   'gui_Singleton',  gui_Singleton, ...
                   'gui_OpeningFcn', @rumex_gui_v5_OpeningFcn, ...
                   'gui_OutputFcn',  @rumex_gui_v5_OutputFcn, ...
                   'gui_LayoutFcn',  [] , ...
                   'gui_Callback',   []);
if nargin && ischar(varargin{1})
    gui_State.gui_Callback = str2func(varargin{1});
end

if nargout
    [varargout{1:nargout}] = gui_mainfcn(gui_State, varargin{:});
else
    gui_mainfcn(gui_State, varargin{:});
end
% End initialization code - DO NOT EDIT


% --- Executes just before rumex_gui_v5 is made visible.
function rumex_gui_v5_OpeningFcn(hObject, eventdata, handles, varargin)
```

```
% This function has no output args, see OutputFcn.
% hObject    handle to figure
% eventdata  reserved - to be defined in a future version of MATLAB
% handles    structure with handles and user data (see GUIDATA)
% varargin   command line arguments to rumex_gui_v5 (see VARARGIN)

% Choose default command line output for rumex_gui_v5
handles.output = hObject;
% Update handles structure
guidata(hObject, handles);



% GLOBALE VARIABLES -----------------------------------------------------
global fname;
global pathname;
global classlist;
global boundlist;

% LOAD START IMAGE AND DISPLAY------------------------------------------
rgb = imread('start.jpg'); imshow(rgb); drawnow;



% --- Outputs from this function are returned to the command line.
function varargout = rumex_gui_v5_OutputFcn(hObject, eventdata, handles)
% varargout  cell array for returning output args (see VARARGOUT);
% hObject    handle to figure
% eventdata  reserved - to be defined in a future version of MATLAB
% handles    structure with handles and user data (see GUIDATA)

% Get default command line output from handles structure
varargout{1} = handles.output;



% IMAGE SELECTION DIALOGUE-----------------------------------------------
```

```
% --- Executes on button press in pushbutton_directory.
function pushbutton_directory_Callback(hObject, eventdata, handles)
% hObject    handle to pushbutton_directory (see GCBO)
% eventdata  reserved - to be defined in a future version of MATLAB
% handles    structure with handles and user data (see GUIDATA)
global currentpath;
global fname,
global pathname;
currentpath = pwd; % SET CURRENT DIRECTORY AS WORKING DIRECTORY
[fname, pathname] = uigetfile({'*.jpg;*.jpeg;*.tif;*.tiff;', ...
    'Image Files (*.jpg,  *.jpeg,  *.tif,  *.tiff)';
    '*.jpg;*jpeg', 'JPG files (*.jpg,  *.jpeg)';...
    '*.tif;*tiff', 'TIFF files (*.tif,  *.tiff)';},...
    'Select image files','MultiSelect','on');
set(handles.pushbutton_training,'Enable','on'); % ENABLE TRAINING SELECTION


% TRAINING DATA SET SELECTION DIALOGUE-------------------------------------
% --- Executes on button press in pushbutton_training.
function pushbutton_training_Callback(hObject, eventdata, handles)
% hObject    handle to pushbutton_training (see GCBO)
% eventdata  reserved - to be defined in a future version of MATLAB
% handles    structure with handles and user data (see GUIDATA)
global currentpath;
global training_fname,
global training_pathname;
cd(currentpath); % GOTO WORKING DIRECTORY
[training_fname, training_pathname] = ...
    uigetfile('*.mat','Select the M-file','MultiSelect','off');
set(handles.pushbutton_classify,'Enable','on'); % ENABLE CLASSIFICATION


% CLASSIFY BUTTON ACTION---------------------------------------------------
% INITIALISES THE CLASSIFICATION OF SELECTED IMAGES
```

```
% --- Executes on button press in pushbutton_classify.
function pushbutton_classify_Callback(hObject, eventdata, handles)
% hObject    handle to pushbutton_classify (see GCBO)
% eventdata  reserved - to be defined in a future version of MATLAB
% handles    structure with handles and user data (see GUIDATA)
global fname;
global pathname;
global training_fname;
global training_pathname;
global out;
global boundlist;
global classlist;
global featlist;
global arealist;
global R_IMG_COORD; global RCOORD;
global PS; global area; global C;

% OPEN SELECTED TRAINING DATA SET
% returns the variables 'patterns' and 'targets' to the workspace
% patterns = sample objects with their features
% targets = class membeship of the sample objects
load (fullfile(training_pathname, training_fname));
procstr = 'Processing';

% OUTPUT DIRECTORY DIALOGUE FOR ANNOTATED CLASSIFIED IMAGES
outpath = uigetdir(pathname,'Select output directory');


% GET NUMBER OF INPUT IMAGES
if iscell(fname)
    [n,m] = size(fname);
else
    m = 1;
end
```

```
% DECLARE OUTPUT VARIABLES
out = []; R_IMG_COORD = []; RCOORD = []; FR = [];
for i=1:m

tic
%     EVALUATE FILENAME
    if iscell(fname)
        thisfile = fname{i};
    else
        thisfile = fname(i,:);
    end

%   PRINT STATUS MESSAGE
    statusmsg = strcat('Processing image - ',...
        num2str(i),'/',num2str(m),': >>',thisfile,'<<');
    set(handles.text_status,'String',statusmsg);drawnow;

%   LOAD CURRENT IMAGE FILE
    rgb = imread(fullfile(pathname, thisfile));

%   GET IMAGE DIMENSION
    [ydim xdim zdim] = size(rgb);

%   SEGMENTATION PARAMETERS DEPENDING ON IMAGE RESOLUTION (SIZE)
%   areathresh = small objects threshold
%   se = size of structure element for image morphology
%   ps = pixelsize in mm
    areathresh = 5000; se = 8; PS = 0.6;
    switch xdim
        case 640
            areathresh = 190; se = 3; PS = 3.0;
        case 1024
            areathresh = 480; se = 4; PS = 1.9;
```

```
        case 1280
            areathresh = 610; se = 5; PS = 1.5;
        case 1600
            areathresh = 1220; se = 6; PS = 1.2;
        case 2271
            areathresh = 2450; se = 7; PS = 0.7;
        case 3264
            areathresh = 5000; se = 8; PS = 0.6;
    end

% PERFORM IMAGE SEGMENTATION
% F = matrix with image objects features
% B = matrix with image objects boundary coordinates
% X = matrix with image objects centroid coordinates
% A = matrix with image objects area
    [F B X A] = A_LHSEG_FE_SCALE_COORD(rgb,areathresh,se);

% CALCULATE CONFIDENCE MASK (CIRLCE) FOR CURRENT IMAGE SIZE
% circle with radius of 97% of image width
% circle has its origin in the image center
% circle consists of 50 vertexes
    cm = circle([ydim/2 xdim/2],xdim/2*.97,50);

% APPLY CONFIDENCE MASK IF SELECTED BY USER
% returns only those objects lying completely inside confidence mask
if get(handles.checkbox_cm,'Value')==1
    [F B X A] = isconfident(F,B,X,A,cm);
end

%   CLASSIFY IMAGE OBJECTS
%   performs maximum likelihood classification
%   classlifier is trained by selected training data set
%   c = vector with calculated object classes
    c = ML(patterns,targets,F');
```

```
% SAVE RESULTS INTO VARIABLES
    featlist{i} = F;
    arealist{i} = A;
    boundlist{i} = B;
    classlist{i} = c;

% CALCULATE MASK FOR EACH CLASS
% ro = rumex obtusifolius
% to = taraxacum officinale
% pm = plantago major
% so = soil
% res = residue
    ro = c == 1; to = c == 2; pm = c == 3; so = c == 4; res = c == 5;

% WRITE NUMBER OF OBJECTS PER CLASS FOR CURRENT IMAGE (i) INTO MATRIX 'out'
    out(i,:) = [sum(ro) sum(to) sum(pm) sum(so) sum(res)];

% GET LIST OF AREA OF RUMOB OBJECTS
    area = A(ro);

% GET RUMEX CENTROID COORDINATES AND TRANSFORM TO IMAGE CENTER
    xc = -(xdim/2); yc = -(ydim/2);
    MM = [1 0 xc;0 1 yc; 0 0 1]; % translation matrix
    XX(:,1) = X(ro,2);
    XX(:,2) = X(ro,1);
    R_IMG_COORD{i} = [XX area]; % SAVE NEW IMAGE COORDINATES
    XX(:,3) = ones(sum(ro),1); % populate with constant z value of 1
    XT = ((MM)*XX')'; % translation
    XT(:,2)=XT(:,2).*-1; % mirror y coordinates
    XT(:,3) = XT(:,3).*i; % write indicator for image in column 3

%   TRANSFORM TO METRIC UNITS AND SAVE COORDINATES INTO CELL
    RCOORD{i} = [XT(:,1:2).*PS area.*PS.*PS XT(:,3)];
```

```
    clear XX;

%   PLOT RESULTS
    axes(handles.axes1);
    h = imshow(rgb);  hold on;
    plotbound2image(B(c==1),'r',2);
    plotbound2image(B(c==2),'b',2);
    plotbound2image(B(c==3),'m',2);
    plotbound2image(B(c==4),'k',2);
    plotbound2image(B(c==5),'y',2);
    plot(cm(:,2),cm(:,1),'w','LineWidth',2);
    hold off;
%   Figure title
    resmsg = strcat('Fig: Result for: ',' >>',thisfile,'<<');
    set(handles.text_result,'String',resmsg);

% PLOT RESULTS FOR IMAGE CLASSIFICATION INTO LISTBOX
    % classified objects
    outstr = num2str(out);
    set(handles.listbox_results,'String',outstr);
    set(handles.listbox_results,'Max',i);
    % object coordinates and area
    outstr_coord = num2str(R_IMG_COORD{i});
    % display results on listbox
    set(handles.listbox_coords,'String',outstr_coord);
    set(handles.listbox_coords,'Max',i);
    drawnow;

%   SAVE ANNOTATED IMAGES
%   Check autosave activation
    if get(handles.checkbox_autosave,'Value')==1
        disp('JETZT')
        FR = getframe(gca);
        mv(i) = FR;
```

```
        [X,Map] = frame2im(FR);
        imwrite(X,fullfile(outpath, strcat(thisfile,'.jpg')),'jpeg');
    end
    toc
end % END OF IMAGE CLASSIFICATION

    %movie2avi(mv,fullfile(pathname, 'mymovie.avi'));
    %avifile(fullfile(pathname, 'mymovie.avi'),'fps',1);
    %movie(mv);

    statusmsg = strcat('Processing finished.');
%   ENABLE EXPORT BUTTONS
    set(handles.pushbutton_export,'Enable','on');
    set(handles.pushbutton_export_coord,'Enable','on');
    set(handles.pushbutton_exp_feat,'Enable','on');
    set(handles.text_status,'String',statusmsg);drawnow;

% LISTBOX FOR CLASSIFICATION RESULTS DISPLAY-------------------------------
% --- Executes on selection change in listbox_results.
function listbox_results_Callback(hObject, eventdata, handles)
% hObject    handle to listbox_results (see GCBO)
% eventdata  reserved - to be defined in a future version of MATLAB
% handles    structure with handles and user data (see GUIDATA)

global fname; global pathname;
global boundlist; global classlist;
global R_IMG_COORD;

% GET SELECTED ITEM NUMBER
    k = get(hObject,'Value');
% LOAD AND DISPLAY RESULTS FOR SELECTED ITEM
    if iscell(fname)
        thisfile = fname{k};
    else
```

```
        thisfile = fname(k,:);
    end

    hold off;
    rgb = imread(fullfile(pathname, thisfile));
    imshow(rgb);
    [ydim xdim zdim] = size(rgb);
    cm = circle([ydim/2 xdim/2],xdim/2*.97,50);
    hold on;

    c = classlist{k}==1;
    B = boundlist{k};
    plotbound2image(B(classlist{k}==1),'r',2);
    plotbound2image(B(classlist{k}==2),'b',2);
    plotbound2image(B(classlist{k}==3),'m',2);
    plotbound2image(B(classlist{k}==4),'k',2);
    plotbound2image(B(classlist{k}==5),'y',2);
    plot(cm(:,2),cm(:,1),'w','LineWidth',2);
    hold off;

    resmsg = strcat('Fig: Result for: ',' >>',thisfile,'<<');
    set(handles.text_result,'String',resmsg);

    outstr_coord = num2str(R_IMG_COORD{k});
    set(handles.listbox_coords,'String',outstr_coord);

% --- Executes during object creation, after setting all properties.
function listbox_results_CreateFcn(hObject, eventdata, handles)
% hObject    handle to listbox_results (see GCBO)
% eventdata  reserved - to be defined in a future version of MATLAB
% handles    empty - handles not created until after all CreateFcns called

% Hint: listbox controls usually have a white background on Windows.
%       See ISPC and COMPUTER.
```

```
if ispc && isequal(get(hObject,'BackgroundColor'),...
        get(0,'defaultUicontrolBackgroundColor'))
    set(hObject,'BackgroundColor','white');
end

% LISTBOX FOR RUMOB COORDINATE DISPLAY-------------------------------------
% --- Executes on selection change in listbox_coords.
function listbox_coords_Callback(hObject, eventdata, handles)
% hObject    handle to listbox_coords (see GCBO)
% eventdata  reserved - to be defined in a future version of MATLAB
% handles    structure with handles and user data (see GUIDATA)

% --- Executes during object creation, after setting all properties.
function listbox_coords_CreateFcn(hObject, eventdata, handles)
% hObject    handle to listbox_coords (see GCBO)
% eventdata  reserved - to be defined in a future version of MATLAB
% handles    empty - handles not created until after all CreateFcns called

% Hint: listbox controls usually have a white background on Windows.
%       See ISPC and COMPUTER.
if ispc && isequal(get(hObject,'BackgroundColor'),...
        get(0,'defaultUicontrolBackgroundColor'))
    set(hObject,'BackgroundColor','white');
end

% EXPORT CLASSIFICATION RESULTS TO EXCEL----------------------------------
% --- Executes on button press in pushbutton_export.
function pushbutton_export_Callback(hObject, eventdata, handles)
% hObject    handle to pushbutton_export (see GCBO)
% eventdata  reserved - to be defined in a future version of MATLAB
% handles    structure with handles and user data (see GUIDATA)
global out;
global fname;
headCell = ...
```

```
    {'Filename','N_RUMOB','N_TAROF/Res.','N_PLAMA','N_SOIL','N_RESID'};
dataCell = num2cell(out);
outCell = [fname' dataCell];
[file,path] = uiputfile('output.xls','Save file name');
xlswrite(fullfile(path, file),[headCell;outCell]);

% EXPORT COORDINATES TO EXCEL-----------------------------------------------
% --- Executes on button press in pushbutton_export_coord.
function pushbutton_export_coord_Callback(hObject, eventdata, handles)
% hObject    handle to pushbutton_export_coord (see GCBO)
% eventdata  reserved - to be defined in a future version of MATLAB
% handles    structure with handles and user data (see GUIDATA)
global R_IMG_COORD; global RCOORD;
headCell = ...
    {'IMG_X','IMG_Y','IMG_AREA','IMG_X_M','IMG_Y_M','AREA','IMG_ID'};
dataCell = [cell2mat(R_IMG_COORD') cell2mat(RCOORD')];
outCell = num2cell(dataCell);
assignin('base','coords',cell2mat(RCOORD'));
[file,path] = uiputfile('coordinates.xls','Save file name');
xlswrite(fullfile(path, file),[headCell;outCell]);



% EXPORT FEATURES TO MATLAB VARIABLE----------------------------------------
% --- Executes on button press in pushbutton_exp_feat.
function pushbutton_exp_feat_Callback(hObject, eventdata, handles)
% hObject    handle to pushbutton_exp_feat (see GCBO)
% eventdata  reserved - to be defined in a future version of MATLAB
% handles    structure with handles and user data (see GUIDATA)
global featlist;
global arealist;
global boundlist;
global classlist;
global RCOORD;
[file,path] = uiputfile('features.mat','Save file name');
```

```
save(fullfile(path, file),...
    'featlist','arealist','boundlist','classlist','RCOORD');




% CHECKBOXES----------------------------------------------------------------
% --- Executes on button press in checkbox_autosave.
function checkbox_autosave_Callback(hObject, eventdata, handles)
% hObject    handle to checkbox_autosave (see GCBO)
% eventdata  reserved - to be defined in a future version of MATLAB
% handles    structure with handles and user data (see GUIDATA)

% Hint: get(hObject,'Value') returns toggle state of checkbox_autosave
get(hObject,'Value')

% --- Executes on button press in checkbox_cm.
function checkbox_cm_Callback(hObject, eventdata, handles)
% hObject    handle to checkbox_cm (see GCBO)
% eventdata  reserved - to be defined in a future version of MATLAB
% handles    structure with handles and user data (see GUIDATA)

% Hint: get(hObject,'Value') returns toggle state of checkbox_cm
```

A_LHSEG_FE_SCALE.m

```
function [feat,B,X,A] = A_LHSEG_FE_SCALE(img,AREA,SE_SIZE)
% IMAGE SEGMENTATION AND FEATURE EXTRACTION
% INPUT VARIABLES
% img = RGB image
% AREA = threshold for small objects
% SE = size of structure element for morphologic image opening
% OUTPUT VARIABLES
% feat = matrix with image objects features
% B = matrix with image objects boundary coordinates
```

```
% X = matrix with image objects centroid coordinates
% A = matrix with image objects area

% SEGMENTATION
% get colour bands
R = img(:,:,1);G=img(:,:,2);B=img(:,:,3);
% calculate intensity image
intensity = R.*0.2989+G.*0.5870+B.*0.1140;
% calculate gradient image
GR = grad(intensity);
% calculate standard deviation image
S = stdfilt(intensity);
% normalize
GR_n = GR/max(max(GR));
S_n = S/max(max(S));
% calculate local homogeneity image
LH = 1-GR_n.*S_n;
% calculate grey level threshhold
ts = mean(mean(LH));
% ts = .97;
% calculate binary image
f = im2bw(LH,ts);
% apply morphological opening
SE = strel('diamond',SE_SIZE);
f = imopen(f,SE);
% remove small objects
f = bwareaopen(f,AREA);
% get object boundaries, ignore holes
[B,L] = bwboundaries(f,8,'noholes');

% FEATURE EXTRACTION
% get number of objects
k = max(max(L));
```

```
% do for all objects
for i=1:k
% calculate object centroid
    for j=1:k
        X(j,1:2) = sum(B{j})./length(B{j});
    end
    m = L == i;
% get object area
    A(i,1) = sum(sum(m));

% calculate object features
% colour features
    feat(i,1) = mean(mean(intensity(m)));
    feat(i,2) = mean(mean(R(m)));
    feat(i,3) = mean(mean(G(m)));
    feat(i,4) = std2(intensity(m));
    feat(i,5) = std2(R(m));
    feat(i,6) = std2(G(m));
% texture features
    feat(i,7) = mean(mean(GR(m)));
    feat(i,8) = mean(mean(S(m)));
    feat(i,9) = mean(mean(LH(m)));
    feat(i,10) = std2(GR(m));
    feat(i,11) = std2(S(m));
    feat(i,12) = std2(LH(m));
end
```

grad.m

```
function g = grad(i)
% Gradient of an Graylevel Image
% using the Sobel Operator

sh = fspecial('sobel');
```

```
sv = sh';
Rx = imfilter(double(i),sh,'replicate');
Ry = imfilter(double(i),sv,'replicate');
% magnitude
g = sqrt(Rx.^2+Ry.^2);
```

circle.m

```
function c = circle(center,radius,NOP)
% calculate circle
% center = origin of circle
% radius = radius of circle
% NOP = number of vertex points
% c = list of circle points

THETA=linspace(0,2*pi,NOP);
RHO=ones(1,NOP)*radius;
[X,Y] = pol2cart(THETA,RHO);
X=X+center(1);
Y=Y+center(2);
c = [X' Y'];
```

isconfident.m

```
function [Fout Bout Xout Aout] = isconfident(F,B,X,A,cm);
% FIND OBJECTS COMPLETELY CONTAINED IN CONFIDENCE MASK (circle, polygon)

% get number of objects
    nPolys = length(B);
% define index variable
    ix = zeros(1,nPolys);
% do for all objects
    for j=1:nPolys
%       get current object boundary
        bnd = B{j};
```

```
%       get number of boundary vertexex within confidence mask
%       if all points are inside, write to index
        in = inpolygon(bnd(:,2),bnd(:,1),cm(:,2),cm(:,1));
        if (sum(in) == length(bnd))
            ix(j) = 1;
        end
    end

%   get all indexed objects
    Bout = B(logical(ix));
    Fout = F(logical(ix'),:);
    Xout = X(logical(ix),:);
    Aout = A(logical(ix'),:);
```

plotbound2image.m

```
function plotbound2image(B,c,w)

for k=1:length(B),
 boundary = B{k};
 plot(boundary(:,2), boundary(:,1), c,'LineWidth',w);
end
```

ML.m and classify_paramteric.m

These scripts are provided by Stork *et al.* (2004) available with their book.

D. Mapping source codes

calc_gis_dbf.m

```
function f = calc_gis_dbf(R,c)
% CREATE XLS TABLE WITH RUMOB OBJECT COORDINATES AND AREA
% BASED ON THE CLASSIFICATION RESULTS USING AFFINE TRANSFORMATION
% R = cell containing n lists with coordinates (n is the number of
% classified images)
% c = list with centroid coordinates of experimental plots in gauss krueger
% the length of c must be n.

% do for each image
for i=1:length(R)
%   get rumob coordinates
    oc = R{i};
%   scale coordinates to metres and area to sqcm
    oc(:,1) = oc(:,1)*.001;
    oc(:,2) = oc(:,2)*.001;
    oc(:,3) = oc(:,3)*.01;
    R{i} = oc(:,1:3);
end

% affine transformation
gk = transform2gk(R,c);
gklist = cell2mat(gk');
Rlist = cell2mat(R');
gklist(:,3) = Rlist(:,3);
f = gklist;
```

```
% export to excell
headCell = {'X','Y','AREA'};
outCell = num2cell(f);
[file,path] = uiputfile('2006_xx_xx_G4_d11_links_gis.xls','Save file name');
xlswrite(fullfile(path, file),[headCell;outCell]);
```

transform2gk.m

```
function gk = transform2gk(l,c);
% AFFINE TRANSFORMATION FROM METRIC IMAGE COORDINATES TO GAUSS-KRUEGER
% l = list of object coordinates as cell array
% c = list of centroid coordinates in gauss krueger
if length(l)~=length(c)
    error('Length of input data must be equal');
end
z = length(l);
% calculate rotation angle
alpha = atan( (c(end,1)-c(1,1))/(c(end,2)-c(1,2)) );
% images were capture on head, therefore rotate at 180 degree
alpha = alpha+pi;
% do for all images
for i=1:z
    % current centroid
    cc = c(i,:);
    % tranformation matrix
    A = [cos(alpha) -sin(alpha) 0; sin(alpha) cos(alpha) 0; cc(1,1) cc(1,2) 1];
    % current image object coordinate list
    ll = l{i};
    % set unique elevation
    ll(:,3) = 1;
    % affine transformation
    gk{i} = (transpose(A)*ll')';
end
```